Journal of Human Evolution 66 (2014) 39–63

Contents lists available at ScienceDirect

Journal of Human Evolution

journal homepage: www.elsevier.com/locate/jhevol

The chronostratigraphy of the Haua Fteah cave (Cyrenaica, northeast Libya)

Katerina Douka [a], Zenobia Jacobs [b], Christine Lane [a], Rainer Grün [c], Lucy Farr [d], Chris Hunt [e], Robyn H. Inglis [f], Tim Reynolds [g], Paul Albert [h], Maxime Aubert [b], Victoria Cullen [a], Evan Hill [e], Leslie Kinsley [c], Richard G. Roberts [b], Emma L. Tomlinson [i,h], Sabine Wulf [j], Graeme Barker [d,*]

[a] Research Laboratory for Archaeology and the History of Art, University of Oxford, Dyson Perrins Building, South Parks Road, Oxford OX1 3QY, UK
[b] Centre for Archaeological Science, School of Earth and Environmental Sciences, University of Wollongong, Wollongong, NSW 2522, Australia
[c] Research School of Earth Sciences, Australian National University, Canberra 0200, Australia
[d] McDonald Institute for Archaeological Research, University of Cambridge, Cambridge CB2 3ER, UK
[e] School of Geography, Archaeology and Palaeoecology, Queen's University Belfast, Belfast BT7 1NN, Ireland
[f] Department of Archaeology, University of York, King's Manor, York YO1 7EP, UK
[g] Department of History, Classics and Archaeology, Birkbeck College, University of London, 26 Russell Square, London WC1B 5DQ, UK
[h] Department of Earth Sciences, Royal Holloway University of London, Egham TW20 0EX, UK
[i] Department of Geology, Trinity College Dublin, Dublin 2, Ireland
[j] GFZ German Research Centre for Geosciences, Section 5.2 – Climate Dynamics and Landscape Evolution, Telegrafenberg, D-14473 Potsdam, Germany

ARTICLE INFO

Article history:
Received 7 December 2012
Accepted 25 October 2013
Available online 12 December 2013

Keywords:
North Africa
Hominin dispersals
Neolithisation
Dating

ABSTRACT

The 1950s excavations by Charles McBurney in the Haua Fteah, a large karstic cave on the coast of northeast Libya, revealed a deep sequence of human occupation. Most subsequent research on North African prehistory refers to his discoveries and interpretations, but the chronology of its archaeological and geological sequences has been based on very early age determinations. This paper reports on the initial results of a comprehensive multi-method dating program undertaken as part of new work at the site, involving radiocarbon dating of charcoal, land snails and marine shell, cryptotephra investigations, optically stimulated luminescence (OSL) dating of sediments, and electron spin resonance (ESR) dating of tooth enamel. The dating samples were collected from the newly exposed and cleaned faces of the upper 7.5 m of the ~14.0 m-deep McBurney trench, which contain six of the seven major cultural phases that he identified. Despite problems of sediment transport and reworking, using a Bayesian statistical model the new dating program establishes a robust framework for the five major lithostratigraphic units identified in the stratigraphic succession, and for the major cultural units. The age of two anatomically modern human mandibles found by McBurney in Layer XXXIII near the base of his Levalloiso-Mousterian phase can now be estimated to between 73 and 65 ka (thousands of years ago) at the 95.4% confidence level, within Marine Isotope Stage (MIS) 4. McBurney's Layer XXV, associated with Upper Palaeolithic Dabban blade industries, has a clear stratigraphic relationship with Campanian Ignimbrite tephra. Microlithic Oranian technologies developed following the climax of the Last Glacial Maximum and the more microlithic Capsian in the Younger Dryas. Neolithic pottery and perhaps domestic livestock were used in the cave from the mid Holocene but there is no certain evidence for plant cultivation until the Graeco-Roman period.

Introduction

The research agenda on North African prehistory is dominated by three major debates: (1) the timing and dispersal routes of modern humans into the region, and whether particular types of lithic assemblage are reliable indicators of their presence (Cremaschi et al., 1998; Mercier et al., 2007; Smith et al., 2007; Garcea, 2010a,

* Corresponding author.
E-mail addresses: katerina.douka@rlaha.ox.ac.uk (K. Douka), zenobia@uow.edu.au (Z. Jacobs), Christine.lane@rlaha.ox.ac.uk (C. Lane), rainer.grun@anu.edu.au (R. Grün), lrf24@cam.ac.uk (L. Farr), c.hunt@qub.ac.uk (C. Hunt), robyn.inglis@york.ac.uk (R.H. Inglis), te.reynolds@bbk.ac.uk (T. Reynolds), pgalbert17@googlemail.com (P. Albert), maubert@uow.edu.au (M. Aubert), victoria.cullen@keble.ox.ac.uk (V. Cullen), ehill08@qub.ac.uk (E. Hill), leslie.kinsley@anu.edu.au (L. Kinsley), rgrob@uow.edu.au (R.G. Roberts), tomlinse@tcd.ie (E.L. Tomlinson), swulf@gfz-potsdam.de (S. Wulf), gb314@cam.ac.uk (G. Barker).

0047-2484/$ – see front matter © 2013 Elsevier Ltd. All rights reserved.
http://dx.doi.org/10.1016/j.jhevol.2013.10.001

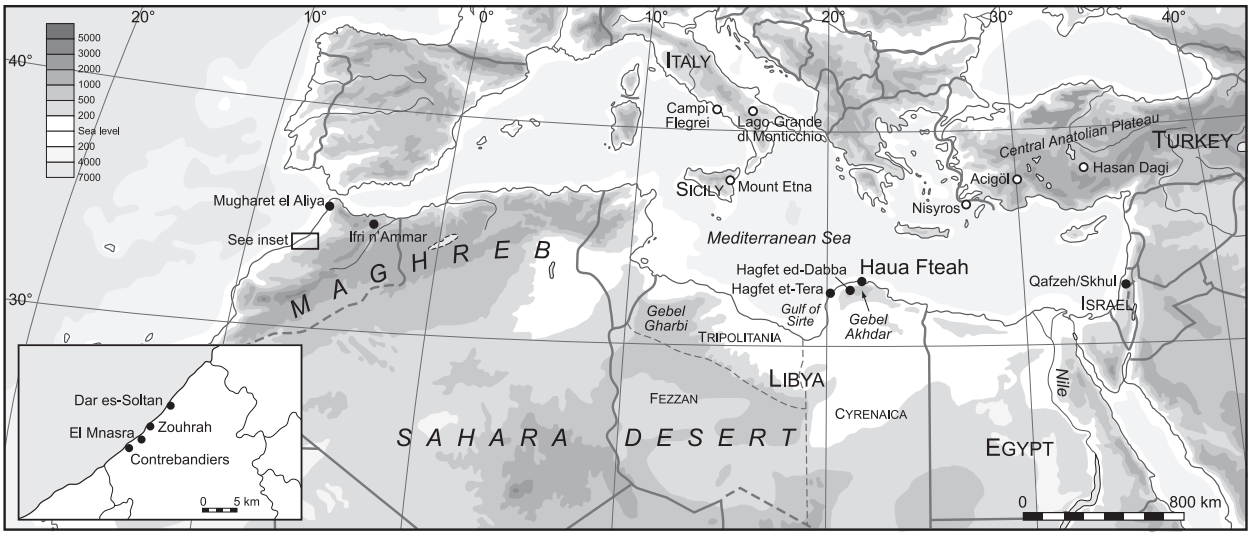

Figure 1. North Africa, showing the location of the Haua Fteah cave together with other sites and places mentioned in the text. Solid circle: archaeological site; open circle: tephra location or palaeoenvironmental site (Drawing: D. Kemp).

2011; Pereira et al., 2010; Wengler, 2010; Hublin and McPherron, 2011; Dibble et al., 2012); (2) how successfully, once established, modern human populations were able to adapt to the major climatic and environmental changes of the Late Pleistocene (Barton et al., 2005, 2007; Bouzouggar et al., 2008; Garcea, 2010b); and (3) the timing and routes of dispersal of plant and animal domesticates in the Early Holocene and the contexts of their use (i.e., by the existing populations of hunter–gatherers and/or by immigrant agricultural populations) (Barker, 2006; Linstädter, 2008; Dunne et al., 2012). The deep (~14 m) sequence excavated by Charles McBurney in the 1950s in the Haua Fteah cave in Cyrenaica, northeast Libya (22°3′5″E/32°53′70″N; Fig. 1) has long been central to all three debates because it spanned the Middle and Late Stone Ages (or Middle and Upper Palaeolithic in European terminology), and the Mesolithic and Neolithic periods. In fact, the sequence remains unique for the whole of North Africa east of the Maghreb (McBurney, 1967). However, though in many respects the excavations and subsequent analyses of material were pioneering for their time, techniques in cave excavation, deep-time radiometric dating and archaeological science more generally have all been transformed in the ensuing sixty years; the context for the renewal of fieldwork at the site in 2007 (Barker et al., 2007, 2008, 2009, 2010, 2012). Here we report the initial results of a comprehensive dating program of the geological and cultural sequences that has been one of the primary objectives of the new project.

History of research

The Haua Fteah is situated about a kilometre from the present-day coast at the foot of the northern escarpment of the Gebel Akhdar ('Green Mountain'), an isolated massif with desert to its west, south and east (Fig. 1). The north-facing entrance of the cave is ~50 m wide and ~20 m high; the interior roofed area measures ~80 m across (Fig. 2). By the end of the final (1955) season, McBurney's trench consisted of three stepped units (Fig. 3): an Upper Trench (our terminology, not his) measuring ~10.0 × 10.0 × 2.0 m deep; a Middle Trench measuring ~7.0 × 6.0 × 5.5 m deep; and a Deep Sounding that was published by McBurney as measuring ~2.5 × 1.5 × 6.5 m deep though in fact (as established in 2012) measured 3.8 × 1.6 × 6.5 m deep, giving a total depth for the excavation of 14.0 m. Sediments were removed in horizontal spits, and stratigraphic layers were then defined from

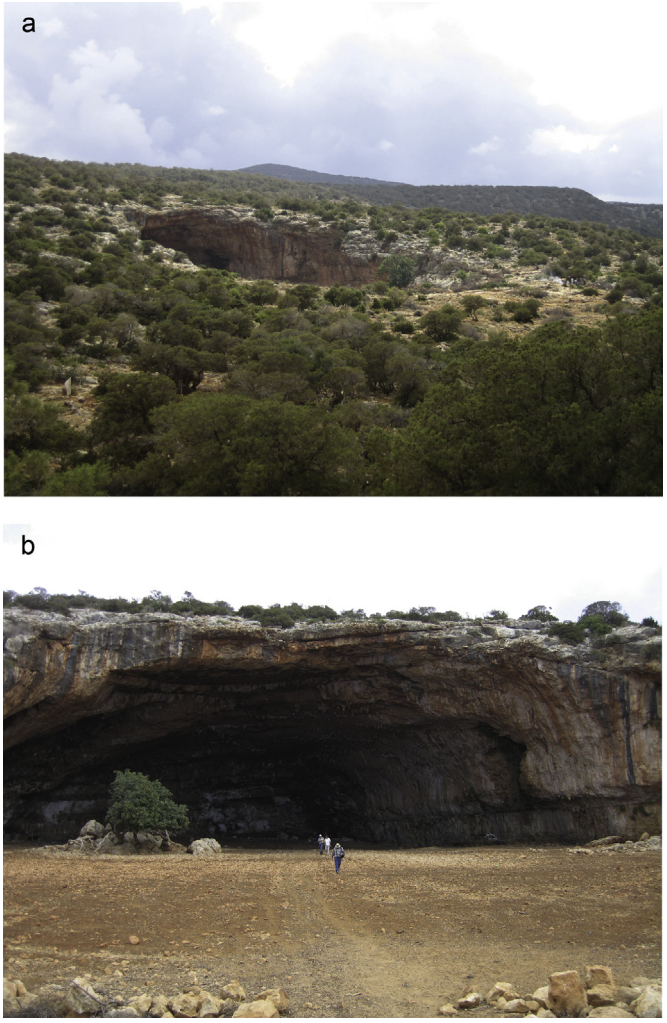

Figure 2. The Haua Fteah cave: (a) looking southwest up to the cave from the coastal plain and (b) looking south across the doline floor into the cave; the standing figures indicate the scale of the cave mouth, which is ~50 m wide and ~20 m high (Photographs: G. Barker).

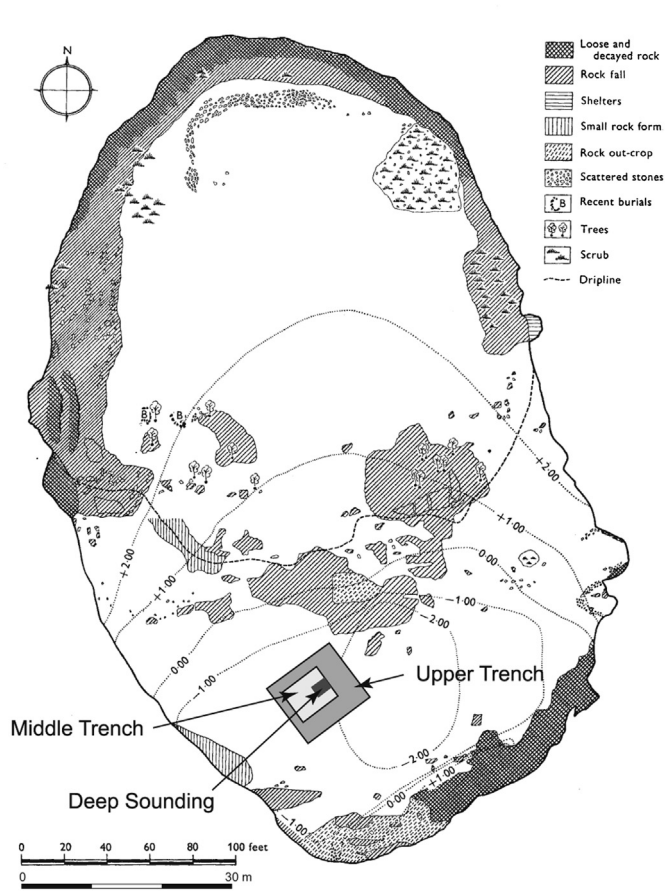

Figure 3. The McBurney (1967) plan, showing the Upper and Middle Trenches (our terms, not McBurney's) and the Deep Sounding. The original plan, including the relative contour heights of the cave surface before excavation, was in feet as shown here, but a metre scale has been added (Drawing: D. Kemp).

the trench walls as the excavations proceeded downwards (Fig. 4). These layers were divided into seven cultural phases, principally on the basis of changes in the stone tool assemblages. Twenty radiocarbon (^{14}C) determinations on wood charcoal and charred bone (treated as charcoal) enabled McBurney to construct a chronology for the upper 6–7 m of the deposit (Callow et al., 1963; Vogel and Waterbolk, 1963, 1967; Supplementary Online Material [SOM] Table S1). Finite ^{14}C ages were obtained for all 20 samples, but the oldest of these were at the then limits of the method, ca. 40 ka BP (thousands of years ago Before Present). Using estimates of sedimentation rates and comparisons with the emerging marine isotopic record, he calculated that the entire deposit probably dated to at least double the age range obtained by ^{14}C for the top 6–7 m, i.e., ca. 80 ka, and that initial occupation probably began during or soon after the Last Interglacial, the beginning of which (MIS 5e) is now dated to 126.0 ± 1.7 ka (Waelbroeck et al., 2008). From comparisons between the published sediment record from the cave and the marine isotope record, Moyer (2003) suggested that the cave's occupation might even go back to 195 ka, the MIS 7 interglacial.

The first phase (Phase A), from the bottom of the Deep Sounding to Layer XXXV at the base of the Middle Trench, contained a flake and blade/flake industry with burins and points. On the evidence of some biface 'trimmers' (in fact from core maintenance) and broken fragments of bifaces, McBurney considered the assemblage to be an "evolved Acheulian-Middle Palaeolithic type" (1967: 78), like the Amudian of Southwest Asia and, with the European Middle and Upper Palaeolithic sequences in mind, proposed the term 'Pre-Aurignacian' given that the Aurignacian was the earliest blade industry of the European Upper Palaeolithic. An age range was estimated of ca. 80–65 ka BP. This was succeeded (Phase B: Layers XXXIV–XXV) by 'Levalloiso-Mousterian' industries, so termed from their broad comparability with these industries in the Levant and Europe, with an age range estimated as ca. 65–40 ka BP. Two human mandibles were found in this part of the sequence, from Layer XXXIII, originally regarded as 'Neanderthaloid' but since confirmed as fully modern human (Hublin, 2000). Layer XXV also contained elements of an industry that continued to Layer XVI (Phase C), characterized by the preferential selection of blanks for the production of blades and with an artefact range that McBurney likened to the European Upper Palaeolithic Gravettian. He named it 'Dabban' after the Cyrenaican cave of Hagfet ed-Dabba where he had found similar material (McBurney, 1960). On the basis of five ^{14}C dates, the age of the Dabban was proposed as ca. 40–15 ka BP (McBurney, 1967). This was succeeded by a microlithic late or final Upper Palaeolithic industry (Phase D, Layers XV–XI) dated to ca. 14–10 ka BP and termed the 'Eastern Oranian' or 'Iberomaurusian' (hereafter 'Oranian') from its similarities with assemblages in the Maghreb. At the junction of the Middle and Upper Trenches (Phase E, Layers X, IX) was a microlithic Mesolithic-type industry (in European terms) with parallels to Capsian assemblages in the Maghreb and, hence, classified as the 'Libyco-Capsian' (hereafter 'Capsian'). Only two ^{14}C dates were obtained from Phase E, both around 7.0 ka BP, but the age of the phase was estimated to be ca. 10.0–7.0 ka BP based on a date of ca. 10.5 ka BP from near the top of the underlying Eastern Oranian layers. Above this was the final prehistoric occupation (Phase F, Layers VIII–IV), with Neolithic pottery and domestic sheep and goats, which was termed 'Neolithic of Libyco-Capsian tradition' (hereafter 'Neolithic') because of similarities in stone tools (the frequency of backed pieces, for example) with the preceding Libyco-Capsian. Four ^{14}C measurements dated this to ca. 7.0–4.7 ka BP. The prehistoric sequence was capped (Phase G) by a substantial boulder-supported structure dating to the Graeco-Roman period (Layers III, II), covered by burnt animal dung and other evidence of animal stalling that dated to recent centuries (Layer I). The cave is still used for stalling sheep and goats, and similar deposits continue to accumulate.

In the course of five seasons of fieldwork, the new project (the Cyrenaican Prehistory Project, or CPP) has removed the backfill deposited in the McBurney trench at the end of the 1955 season, cleaned and recorded the original sections using the single-context stratigraphic recording system, cut 30 × 30 cm column samples from the ground surface to the base of the Deep Sounding for sedimentological and palynological analysis, and is excavating two new trenches down the side of the Middle Trench (Trench M) and Deep Sounding (Trench D) to provide new data about the sedimentary and cultural sequences, and the climatic and environmental contexts in which they developed (Fig. 5). All excavated sediment is being washed and screened down to 2 mm to collect suites of artifactual and bioarchaeological data that will enable the project to test the robustness of McBurney's arguments about the cultural phases he defined and the timing and character of the transitions between them. The faces of the McBurney trench are well preserved, with many of the original aluminium labels still in place, enabling the new stratigraphies to be tied to and compared with McBurney's published stratigraphies. The sedimentary and cultural sequences discussed in this paper come from the Upper and Middle Trenches and very top of the Deep Sounding. The main fill of the latter was only cleared in 2012 on the resumption of fieldwork after the 2011 civil conflict and the recording and dating of its sediments are in progress.

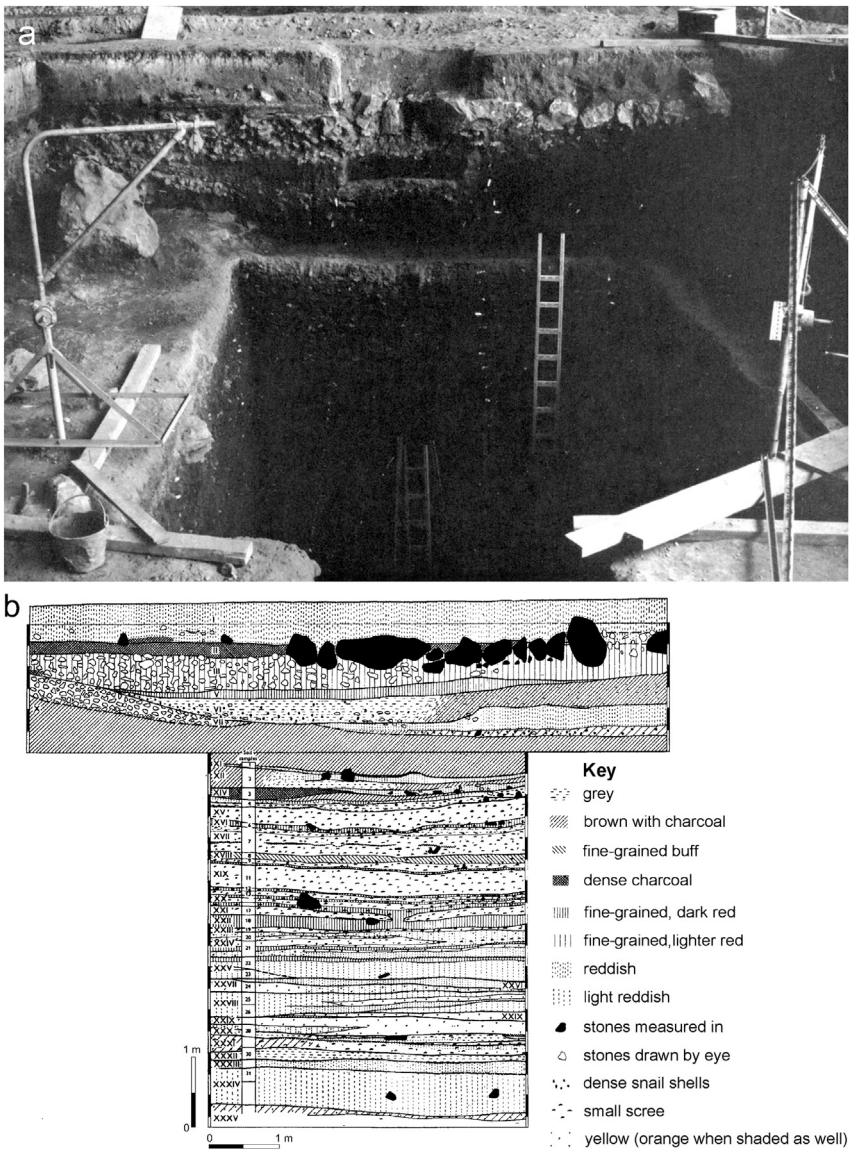

Figure 4. The McBurney trench in 1955: (a) "general view on completion of the operation" (McBurney caption) looking west to the east-facing sections of the Upper and Middle Trenches (McBurney, 1967: plate XXXX, photograph: R. Inskeep). The Upper Trench section measures ~10 m in length, the Middle Trench section measures ~6 m. The large boulder visible near the top of the north-facing section of the Middle Trench, immediately below the metal base frame of the crane, is also visible in the re-excavated face shown as Fig. 5b, and in the CPP drawing of the same section shown as Fig. 6. (b) The stratigraphy of the east-facing sections of the Upper and Middle Trenches as recorded by R. Inskeep in 1955 (McBurney, 1967: Fig. 1.4), together with McBurney's stratigraphic key. The Deep Sounding is not shown. The large boulders in the upper section relate to a Graeco-Roman structure. The Arabic numbers refer to the spits in which the trenches were excavated, the Roman numerals to the stratigraphic layers identified during and after excavation. The use of the spit system has resulted in uncertainties regarding the stratigraphic distributions of archaeological material: Layer XXV, for example, was identified by McBurney as transitional between the Levalloiso-Mousterian and Dabban phases of occupation, and contained material of both types of assemblage. As the figure shows, it was excavated in two spits (23 and 23), the upper spit spanning two distinct stratigraphic units.

Sedimentary processes, facies and environmental interpretations

Five main sedimentary facies have been recognised in the sediments exposed in the Upper and Middle Trenches on the basis of field observations, bulk sedimentological analyses (particle size, calcium carbonate, loss-on-ignition, magnetic susceptibility) and micromorphology (Inglis, 2012; Fig. 6 and SOM Figs. S1–3). Example photomicrographs of the main sediment types as observed micromorphologically are shown in Fig. 7. The bulk sediment analyses are being published separately. They consist of combinations of five main types of sediment: silts and silty clays, éboulis, diamicts, calcite layers, and anthropogenic deposits, reflecting a variation over the long and short term of sedimentary processes and depositional material. The fine sediment material is generally reddish in colour, consistent in character with the terra rossa soil material on the surrounding hillsides, suggesting that this is a key source of sediment throughout the sequence, variously from aeolian transportation or colluvial movements (Hunt et al., 2010), as is common in many Mediterranean caves (e.g., Karkanas, 2001; Woodward and Goldberg, 2001). The layers vary in colour from deep red to lighter orange/buff, with the darkest red layers compact and clay-rich. This variation in colour and texture probably reflects differences in source material. The restriction and clarity of most layer boundaries suggest that the sediments have not undergone significant post-depositional alteration such as leaching or major bioturbation following their burial, which could alter their oxidation state and therefore colour (Taylor, 1982; Bridges, 1997).

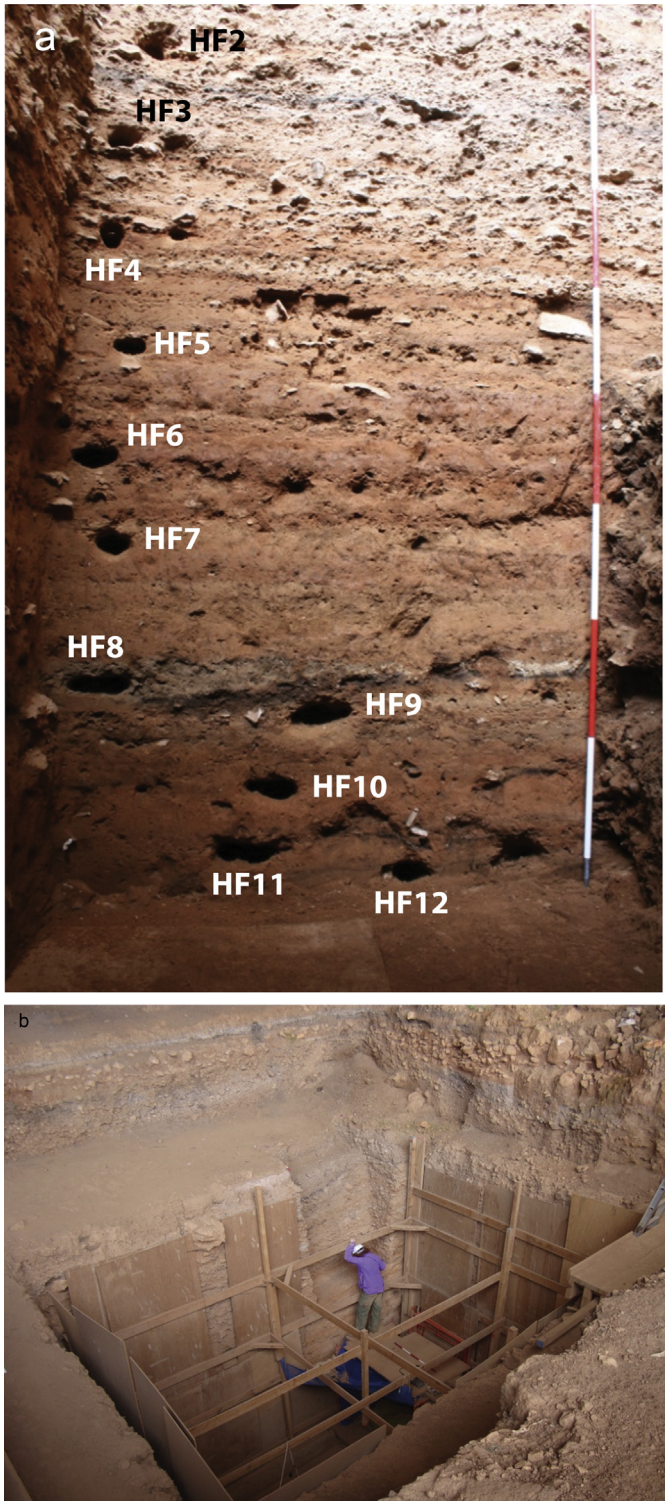

Figure 5. The new (CPP) excavations in the Haua Fteah: (a) the eastern part of the north-facing section of the Middle Trench, looking south; the visible holes are the locations of OSL tubes; scale in 0.5 m divisions: (b) looking southwest across the Middle Trench to the Trench M excavation in 2012; the second plywood sheet to the left of the standing figure covers the part of the Middle Trench wall shown in the left image; the north-facing and east-facing walls of the Upper Trench are visible in front and to the right (compare the latter with the same face in 1955: Fig. 4a). The large boulder near the top of the north-facing section of the Middle Trench, between the two plywood sheets to the left of the standing figure, is visible in the 1955 photograph shown as Fig. 4a (Photographs: G. Barker).

Similarly, the more clayey layers likely reflect clayey sediment source material, rather than the in situ translocation and concentration of clay down profile in horizons (as evidenced by the general lack of clay void coatings that could otherwise attest to the illuviation of clays down profile after the deposition of the unit [Goldberg, 1992]). Where present, these coatings were restricted to the 1–2 cm under sediment layers interpreted as potential mass flows of muddy material, indicating that their formation was related to the short duration in which the overlying unit was deposited (Inglis, 2012).

Lying at the base of the Middle Trench, and representing the deepest part of the stratigraphy discussed in this paper, Facies 5 (at ~7.5–6.5 m depth below the present ground surface, but basal depth currently unknown) consists of red-orange silt layers interpreted as redeposited soil material reworked primarily from the immediate area of the cave but also potentially from further afield, as well as the recycling of sediment already within the dry shelter through aeolian processes. Such deposition was interrupted with rare inwash events that transported more clay-rich soil material from the surrounding hillsides into the shelter. These layers are interspersed with a number of burning features, 0.5–1.0 m wide, one of which has been interpreted as a hearth with multiple ash dumping episodes through micromorphological analysis (Fig. 7a).

Facies 4 (at ~6.0–6.5 m depth) consists of silty greyish sediments and éboulis. The increased physical weathering of the bedrock which produced this éboulis suggests a period of significant cooling, with rare, thin washes of clay-rich soil material redeposited from the surrounding hillside and identified through micromorphological observations (Fig. 7b). This facies is capped by a burning event (CPP Contexts 513 and 535), interpreted by McBurney as an 'immense hearth' (McBurney, 1967) that is heavily-weathered, suggesting its relatively prolonged exposure as a surface (Inglis, 2012).

Facies 3 (at ~4.0–6.0 m depth) consists of dense reddish clay-rich fabrics alternating with lighter-coloured silty clay fabrics, respectively reflecting colluvial inwash and aeolian deposition. Micromorphological observation identified colluvial reworking of potentially aeolian-derived deposits, probably from within the shelter, towards the base of the facies. Towards the top of the facies, clay-rich layers (Fig. 7c) interpreted as inwash increased in frequency, particularly prominent at the layers corresponding to McBurney's Layer XXV. This increase was accompanied by the sporadic occurrence of increasingly thick éboulis lenses produced by greater physical weathering, suggestive of cooler periods. There are also distinct layers of calcite concretion (Fig. 7d) suggestive of periods of increased water dripping or flowing onto the sediments (Macphail and Goldberg, 1999). This could possibly reflect periods of relatively increased precipitation in the local environment (Pickering et al., 2007), although the potential mobility of carbonate through the profile also makes it possible that these horizons may have formed below the cave surface at a later point. The overall interpretation of the facies was one of variable depositional environments that became more markedly different to the top of the facies, potentially in response to punctuated periods of increasing landscape destabilisation and increasing cold.

Facies 2 (at ~2.0–4.0 m depth) consists of silty greyish sediments and éboulis similar to but thicker than those of Facies 4, and containing a series of thick, red clay lenses. This facies contains a visible lens of volcanic tephra (Context 426; see below, Tephrochronology). Many of these sediments appear to have accumulated in a period of increased physical weathering, potentially as a response to a prolonged cold period that was sustained for a significantly longer period than those represented by the thin éboulis layers in the top of Facies 3. Whilst full micromorphological analysis was not carried out within this facies because of the technical difficulty of sampling such coarse-grained deposits, the

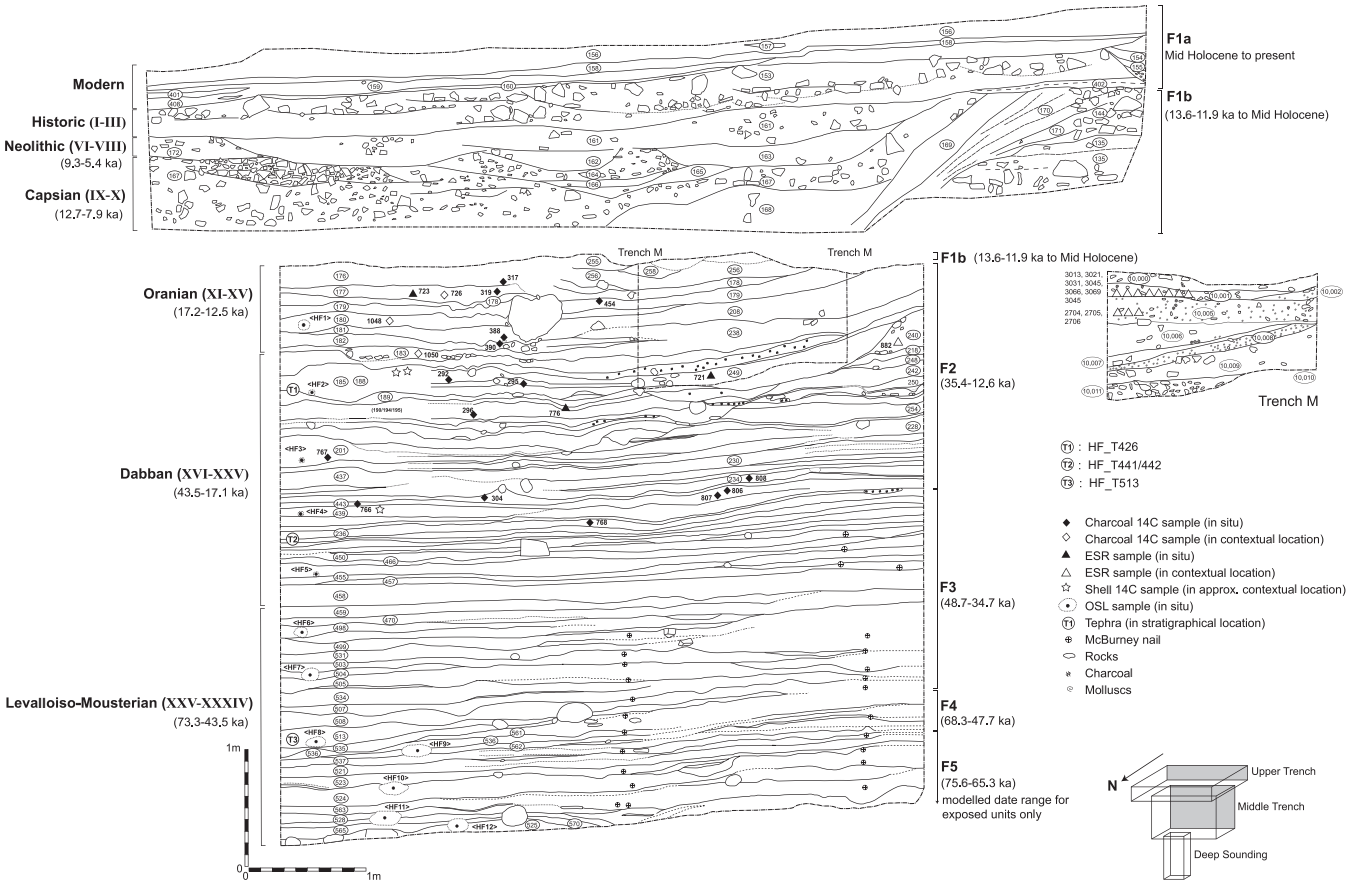

Figure 6. The upper 7.5 m of the McBurney trench (north-facing section), showing the stratigraphic contexts or discrete units defined by the CPP (circled numbers), the McBurney layers and cultural phases, the five sedimentary facies defined by the CPP (the base of Facies 5 is currently unknown), the location of the main series of dated samples used in the Bayesian modelling, and the modelled dates for the cultural sequence (left) and facies (right). See also SOM Figures S1–3 for the other faces of the trench and the other sample locations. Trench M is the new trench being excavated down the side of the Middle Trench, the stratigraphy of which up to the end of excavation in 2010 is shown on the right of the main section drawing (Drawings: L. Farr).

sustained high magnetic susceptibility values of the fine material may reflect episodes of landscape degradation that caused the sporadic transport of well-developed soil material from the surrounding hillsides into the shelter during inwash events. The latter can be traced in the sections, and were confirmed through limited micromorphological analysis, although these values may also have been raised by extended periods of surface exposure and weathering, as well as an increased anthropogenic influence in these levels. The part of Facies 2 that lies within the new (Trench M) excavations also includes a large channel, presumably cut by a particularly violent inwash event, or series of such events, mixed with rockfall.

Facies 1b (at ~1.0–2.0 m depth) consists of greyish-red silty diamict layers, interpreted as inwash events carrying soil material into the cave from the surrounding hillsides, interbedded with éboulis derived from roof spalling and debris avalanches and mixed with anthropogenic material (Hunt et al., 2010). Facies 1a (0.0–1.0 m depth) consists of red diamicts interpreted as mudflows and large inwash events interbedded with abundant anthropogenic material including midden and stabling (penning and dung-burning) deposits below and especially above the Graeco-Roman structure. The inwash events also change in character from the small-scale flows of sediment from potentially aeolian and less pedogenically-altered sources in Facies 1b to large-scale mudflows of external soil material interpreted as the relocation of eroding ploughsoils, a change that began shortly before the construction of the Graeco-Roman structure.

Evidence of micro-scale bioturbation by soil microfauna, in the form of granular micro-fabrics visible in thin section, is abundant, but the macro-scale clarity of the layer boundaries suggests that such bioturbation may have been restricted to the top few exposed centimetres of layers, largely ceasing after burial. Burrows visible in the profiles indicate that bioturbation by larger fauna such as mole rats is likely to have had a more disruptive impact, potentially mixing younger and older sediments and fine materials, such as charcoal and glass shards, and incorporating 1950s backfill into adjacent ancient deposits. The occurrence of large amounts of rockfall, especially in Facies 4 and 2, may have allowed post-depositional downward movement of sediments and fine materials in cracks between the rocks as a result of human and animal trampling. Colluvial inwash and mass mudflow events, such as the one observed in Trench M, can truncate deposits, and mix sediments and fine materials of different ages, from inside and outside the cave, together during transportation. The potential impacts of these bioturbation processes on the dating program are discussed below.

The multi-method dating study

A multi-method dating approach was adopted involving accelerator mass spectrometry (AMS) radiocarbon (^{14}C) dating, cryptotephra investigations, optically stimulated luminescence (OSL) and electron spin resonance (ESR) techniques; an extensive series of samples has been analysed (Fig. 6 and SOM Figs. S1–3). The target

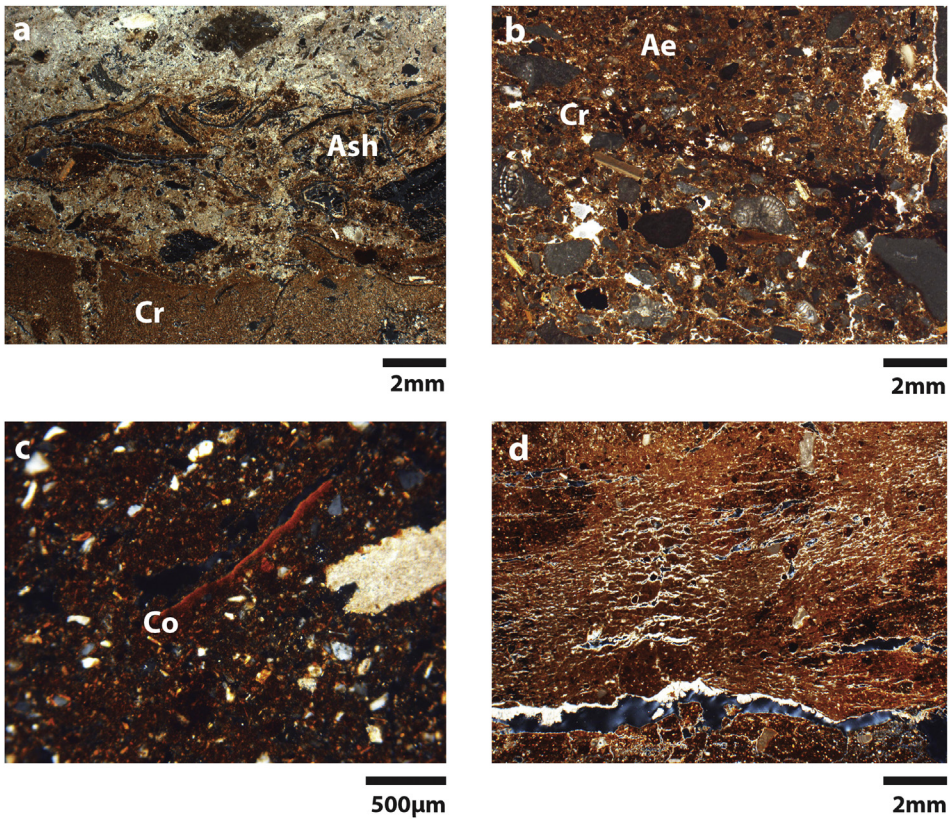

Figure 7. Photomicrographs showing the main sediment types within the Haua Fteah as observed through micromorphology: (a) Sample HF09-2155, Microfabrics 3 and 4, XPL: detail of burning event in Facies 5 showing interpreted ash dump (Ash) over crust of clay-rich (Cr) material potentially laid down by an inwash of clay-rich material during a period of hearth disuse; (b) Sample HF08/09-2033, Microfabric 3, PPL (plane polarized light): fine homogeneous silt (Ae) with sand-sized limestone éboulis interpreted as the result of continued aeolian reworking of material within the cave and in the immediate cave surroundings; note thin clay crust (Cr) interpreted as a small-scale wash event – larger lenses in Facies 4 visible in section are interpreted as larger scale wash events, perhaps from outside the cave; (c) Sample HF08-762, Microfabric 1, XPL: clay-rich fabric with stipple-speckled to mosaic b-fabric (the appearance of the fine material under cross polarised light) interpreted as reworked soil material deposited in a mass colluvial movement; clay coating to vegetal void (Co); (d) Sample HF09-2621, Microfabric 3, XP: calcite-cemented unit interpreted as resulting from water dripping or flowing onto sediments; precipitation of crystals in voids has produced platy microstructure similar to that observed in fabrics that have undergone freeze-thaw processes (Analysis by R. Inglis; descriptive terminology following Stoops, 2003).

dating event of the different methods employed is different, and it is important to keep this in mind when comparisons among methods are made and their accuracy interpreted (SOM 3: Dating program). Summaries of the methods and results of each dating technique are provided in the following sections, with further detail provided as SOM.

Radiocarbon (^{14}C) dating

The original ^{14}C dates obtained by McBurney were made on wood charcoal and charred bone (SOM Table S1) (Callow et al., 1963; Vogel and Waterbolk, 1963, 1967). We report here the results of 96 new AMS ^{14}C measurements obtained since 2007 (Table 1): 64 on charred – partly combusted – plant material of wood charcoal, charred seeds, or pine cone scales, all referred to, hereafter, as charcoal; 28 on terrestrial snails and four on marine shell. Thirty-six ^{14}C measurements were produced at the Oxford Radiocarbon Accelerator Unit (ORAU), 52 in Belfast and eight by Beta Analytic.

The charred plant material typically comprises ~60–90% carbon and at least some components of it appear 'inert' (i.e., resistant to inorganic chemical or biologically mediated oxidation, especially in arid depositional environments). The samples were collected in situ from the cleaned faces of the Upper and Middle Trenches as well as from the newly-opened Trench M. Prior to submission for dating, taxonomic identification of the charred material was undertaken by Caroline Cartwright (British Museum) based on microscopic characteristics (e.g., internal and external physical structure and diagnostic anatomical features revealed through standard techniques of light microscopy) (see also Barker et al., 2008). The ORAU and Beta Analytic charcoal samples were dated using the standard Acid–Base–Acid (ABA) protocol (Brock et al., 2010), as were the five wood charcoal samples dated at Belfast (UBA-16129, UBA-16131–34). The remaining samples dated in Belfast (all cones of *Pinus* sp.) were cleaned using an acid wash only. Some of the material submitted to ORAU was badly preserved and a high rate of failure was observed: ~50% of samples initially submitted for dating did not survive pretreatment and had very low C yield. The carbon content of the samples for which dates were obtained also varied, from 50 to 72% in 25 of the samples to 30–43% in three and just 13–18% in the remaining three samples. The majority of results for the charcoal samples span from the historic period to 49 ka (^{14}C) BP, but five samples yielded very young results, between AD 1650 and AD 1950 when calibrated. These clearly represent intrusions in the stratigraphic column from the modern levels of the site, possibly incorporated during the filling of McBurney's trenches.

Three marine shells (*Columbella rustica*) from the 1952 excavations, held in the McBurney Archive (Museum of Archaeology and Anthropology, University of Cambridge), were dated by the ORAU, producing four results (one sample was dated twice as an internal laboratory check). The shells were intentionally perforated with a punch on the last whorl (E1–2 position of Taborin's system: Taborin, 1993) to create beads. One is from McBurney's Layer XIV–XV, one is from Layer XX, and one is of uncertain provenance, labelled simply '8′–8′6′ depth (Red II)' but most likely associated

Table 1
Radiocarbon determinations for the Haua Fteah obtained by the Cyrenaican Prehistory Project, with approximate correlations with McBurney layers.

Laboratory code	Age	±	Calibrated BP (95.4%)		$\delta^{13}C$	%C	Material	Species	CPP context	Sample ID	Trench	McBurney layer	Comment
			From	To									
OxA-18710	1688	25	1700	1530	−22.2	54.0	Charcoal	*Juniperus* sp.	126	HF 190	E-facing UT	III	Mix of charcoal with sediment. A few pieces were used.
OxA-18673	6917	31	7830	7670	−26	65.3	Charcoal	*Rhus* cf. *tripartita*	131	HF 209	E-facing UT	VI	Mix of charcoal with sediment. Twelve charcoal fragments were selected. Humics.
OxA-18674	6505	33	7490	7320	−25.8	37.7	Charcoal	*Ephedra* sp.	132	HF 238	E-facing UT	VIII	Mix of orange–brown sediment and very small pieces of charcoal. Humics.
OxA-18675	5759	28	6650	6480	−25.9	71.6	Charcoal	*Zygophyllum* sp.	129	HF 243	E-facing UT	VI, V or III	About 20 small pieces of charcoal covered in orange brown sediment were used. Humics.
OxA-18676	5462	30	6310	6200	−25.7	55.3	Charcoal	*Zygophyllum* sp.	129	HF 243	E-facing UT	VI, V or III	About 20 small pieces of charcoal covered in orange brown sediment were used. Humics.
OxA-18794	5521	32	6400	6280	−24.9	28.8	Charcoal	*Zygophyllum* sp.	129	HF 243	E-facing UT	VI, V or III	Remaining material from above was used. Very small pieces of charcoal.
OxA-18677	6115	31	7160	6890	−24.9	15.6	Charcoal	*Suaeda* sp.	131	HF 244	E-facing UT	VI	Mix of charcoal with sediment. Seven charcoal pieces were selected. Low C yield.
OxA-18678	12,360	50	14,900	14,050	−24.7	13.0	Charcoal	*Juniperus* sp.	136	HF 254	E-facing UT	X	Two large charcoal pieces were dated. Low C yield.
OxA-18795	12,750	50	15,580	14,760	−23.6	43.3	Charcoal	*Cupressus* sp.	186	HF 292	N-facing MT	XV–XIV	Mix of charcoal with sediment. Humics.
OxA-18796	13,190	50	16,630	15,390	−24.0	49.0	Charcoal	*Pistacia* sp.	187	HF 295	N-facing MT	XV–XIV	Small (<1 mm) charcoal in sediment.
OxA-18836	170	25	290	modern	−22.0	63.5	Charcoal	*Cupressus* sp.	194	HF 296	N-facing MT	XVII–XVI	One charcoal piece was selected
OxA-18797	26,850	130	31,420	31,060	−23.5	55.2	Charcoal	*Juniperus* sp.	207	HF 304	N-facing MT	XX	Small charcoal, <2 mm.
OxA-19184	9425	40	10,760	10,560	−25.4	59.8	Charcoal	*Juniperus* sp	176	HF 317	N-facing MT	X	Mix of charcoal with sediment. Humics.
OxA-19158	9740	45	11,250	10,890	−23.9	63.9	Charcoal	*Juniperus* sp	177	HF 319	N-facing MT	XI–X	Mix of charcoal with sediment. Humics.
OxA-19028	6413	32	7420	7270	−23.9	58.2	Charcoal	*Rhus* sp. *tripartita*	132	HF 380	S-facing UT	VIII	Mix of charcoal with sediment. Humics.
OxA-19185	12,395	50	14,950	14,100	−21.2	55.2	Charcoal	*Juniperus* sp.	181	HF 388	N-facing MT	XIII–XII	Mix of charcoal with sediment. Humics.
OxA-19186	12,430	50	14,980	14,130	−20.9	32.3	Charcoal	*Juniperus* sp.	182	HF 390	N-facing MT	XIII–XII	Larger charcoal shards were used.
OxA-19029	11,795	45	13,790	13,450	−23.1	69.1	Charcoal	*Pinus* sp.	238	HF 437	E-facing MT	XII	One discreet charcoal shard was used.
OxA-19187	12,260	45	14,800	13,920	−22.3	54.5	Charcoal	*Pinus* sp.	238	HF 438	E-facing MT	XIV	Mix of charcoal with sediment. Larger charcoal fragments were used.
OxA-19030	11,160	45	13,220	12,850	−23.9	58.0	Charcoal	*Juniperus* sp.	179	HF 454	N-facing MT	XI	Mix of charcoal with sediment. Larger charcoal fragments were used.
OxA-19188	12,040	65	14,060	13,730	−22.3	56.3	Charcoal	*Pinus* sp.	238	HF 458	E-facing MT	XIV	Mix of charcoal with sediment. Larger charcoal fragments were used.
OxA-19571	18,720	100	22,630	22,030	−22.6	18.3	Charcoal	*Rhus* sp.	244	HF 464	E-facing MT	XVII	Mix of charcoal with sediment. Larger charcoal fragments were used. Low C yield.
OxA-19189	13,360	55	16,840	15,900	−23.6	52.8	Charcoal	*Rhus* sp.	240	HF 467	E-facing MT	XVI–XV	Mix of charcoal with sediment. Larger charcoal fragments were used.
OxA-22161	9840	60	11,410	11,150	−26.0	59.6	Charcoal	n/a	177	HF 726	N-facing MT	X	Mix of charcoal with sediment.
OxA-22162	27,900	210	32,790	31,480	−24.0	63.8	Charcoal	n/a	443	HF 766	N-facing MT	XX–XIX	Mix of charcoal with sediment. Five small fragments were used.
OxA-22163	101	29	270	10	−25.2	65.8	Charcoal	n/a	201	HF 767	N-facing MT	XVIII–XVII	
OxA-22164	26,120	170	31,140	30,490	−24.7	66.2	Charcoal	n/a	246/236	HF 768	N-facing MT	XXII–XXI	
OxA-22165	229	27	310	modern	−24.2	58.3	Charcoal	n/a	465	HF 806	N-facing MT	XX	Five small fragments were used.
OxA-22166	224	27	310	modern	−22.2	58.6	Charcoal	n/a	465	HF 807	N-facing MT	XX	Five small fragments were used.
OxA-22232	135	26	280	0	−22.3	63.8	Charcoal	n/a	234	HF 808	N-facing MT	XX	Single charcoal fragment was used.
OxA-22137	10,900	45	12,920	12,630	−23.2	61.1	Charcoal	n/a	180	HF 1048	N-facing MT	XII	
OxA-22138	11,855	50	13,850	13,480	−23.5	54.7	Charcoal	n/a	183	HF 1050	N-facing MT	XIII	
UBA-16129	32,656	164	37,850	36,610	−22.1	n/a	Charcoal	n/a	236	S2199	W-facing MT	XXII, XXI or XXB	
UBA-16131	41,658	367	45,790	44,540	−24.6	n/a	Charcoal	n/a	494	S2254	W-facing MT	XXV	
UBA-16132	32,766	145	38,070	36,680	−23.8	n/a	Charcoal	n/a	236–441	S2282	W-facing MT	XXII, XXI or XXB	
UBA-16133	38,085	362	43,160	42,010	−23.6	n/a	Charcoal	n/a	506	S2475	W-facing MT	XXIX	
UBA-16134	48,571	1036	51,020	46,700	−26.0	n/a	Charcoal	n/a	521	S2534	W-facing MT	XXXIV–XXXIII	

Beta-299214	10,200	50	12,090	11,700	n/a	n/a	Charred plant	n/a	10,001 (spit 3)	HF0910001PL	M	XIII–XI	
Beta-299215	10,360	50	12,420	12,030	n/a	n/a	Charred plant	n/a	10,002 (spit 1)	HF0910002V	M	XIII–XI	
Beta-299216	11,870	50	13,870	13,480	n/a	n/a	Charred plant	n/a	10,004 (spit 1)	HF0910004PH	M	XIII–XI	
Beta-299217	12,190	50	14,220	13,830	n/a	n/a	Charred plant	n/a	10,006 (spit 3)	HF1010006RO	M	XIII–XI	
Beta-299218	12,140	50	14,160	13,820	n/a	n/a	Charred plant	n/a	10,007	HF1010007PH	M	XIV–XIII	
Beta-299219	12,110	50	14,130	13,800	n/a	n/a	Charred plant	n/a	10,008	HF1010008IP	M	XIV	
Beta-299220	12,310	50	14,890	13,980	n/a	n/a	Charred plant	n/a	10,009 (spit 7)	HF1010009PH	M	XIV	
Beta-299221	12,030	50	14,030	13,750	n/a	n/a	Charred plant	n/a	10,001 (spit 2)	HF1010011PH	M	XIV	
UBA-18726	12,343	57	14,900	14,030	−26.9	n/a	Charred plant	*Pinus* sp. (cones)	10,006 (spit 1)	06/01-1	M	XIII–XI	
UBA-18727	12,369	72	14,940	14,040	−25.3	n/a	Charred plant	*Pinus* sp. (cones)	10,006 (spit 1B)	06/01B-2	M	XIII–XI	
UBA-18728	12,209	56	14,500	13,830	−24.6	n/a	Charred plant	*Pinus* sp. (cones)	10,006 (spit 2A)	06/02A-2	M	XIII–XI	
UBA-18729	12,220	70	14,560	13,820	−24.5	n/a	Charred plant	*Pinus* sp. (cones)	10,006 (spit 2B)	06/02B-3	M	XIII–XI	
UBA-18730	12,420	61	14,990	14,120	−26.0	n/a	Charred plant	*Pinus* sp. (cones)	10,006 (spit 2A)	06/02A-4	M	XIII–XI	
UBA-18731	12,384	57	14,940	14,080	−25.6	n/a	Charred plant	*Pinus* sp. (cones)	10,006 (spit 2B)	06/02B-5	M	XIII–XI	
UBA-18732	12,280	59	14,870	13,920	−25.7	n/a	Charred plant	*Pinus* sp. (cones)	10,007 (spit 2B)	07/02B-	M	XIV–XIII	
UBA-18733	12,333	57	14,900	14,010	−22.9	n/a	Charred plant	*Pinus* sp. (cones)	10,008 (spit 2B)	08/02B-1	M	XIV	
UBA-18734	12,397	73	14,980	14,070	−25.5	n/a	Charred plant	*Pinus* sp. (cones)	10,008 (spit 2B)	08/02B-2	M	XIV	
UBA-18735	12,515	69	15,090	14,200	−23.2	n/a	Charred plant	*Pinus* sp. (cones)	10,009 (spit 1A)	09/01A-2	M	XIV	
UBA-18736	12,661	63	15,480	14,550	−21.2	n/a	Charred plant	*Pinus* sp. (cones)	10,009 (spit 1B)	09/01B-3	M	XIV	
UBA-18737	12,466	60	15,030	14,160	−25.2	n/a	Charred plant	*Pinus* sp. (cones)	10,009 (spit 1A)	09/01A-4	M	XIV	
UBA-18738	12,450	55	15,010	14,150	−29.7	n/a	Charred plant	*Pinus* sp. (cones)	10,009 (spit 1B)	09/01B-4	M	XIV	
UBA-18739	12,548	55	15,130	14,230	−22.6	n/a	Charred plant	*Pinus* sp. (cones)	10,009 (spit 1B)	09/01B-5	M	XIV	
UBA-18740	12,322	62	14,900	14,000	−20.4	n/a	Charred plant	*Pinus* sp. (cones)	10,009 (spit 2A)	09/02A-5	M	XIV	
UBA-18741	12,329	55	14,900	14,010	−23.5	n/a	Charred plant	*Pinus* sp. (cones)	10,009 (spit 2A)	09/02A-6	M	XIV	
UBA-18742	12,236	55	14,540	13,870	−27.5	n/a	Charred plant	*Pinus* sp. (cones)	10,009 (spit 2B)	09/02B-7	M	XIV	
UBA-18743	12,380	56	14,930	14,070	−26.6	n/a	Charred plant	*Pinus* sp. (cones)	10,011 (spit 2A)	11/02A-1	M	XIV	
UBA-18744	12,266	56	14,840	13,910	−23.9	n/a	Charred plant	*Pinus* sp. (cones)	10,011 (spit 2A)	11/02A-2	M	XIV	
UBA-18697	12,854	57	15,890	14,970	−9.6	n/a	Land snail	*Helix melanostoma*	10,006	ARHC06S1-A	M	XIII–XI	
UBA-18698	12,855	55	15,890	14,970	−12.1	n/a	Land snail	*Helix melanostoma*	10,006	ARHC06S2-A	M	XIII–XI	
UBA-18699	13,708	60	17,030	16,660	−12.3	n/a	Land snail	*Helix melanostoma*	10,008	ARHC08S1-A	M	XIV	
UBA-18700	12,486	65	15,060	14,170	−12.0	n/a	Land snail	*Helix melanostoma*	10,008	ARHC08S2-A	M	XIV	
UBA-18701	12,933	56	16,140	15,060	−16.5	n/a	Land snail	*Helix melanostoma*	10,009	ARHC09S-A	M	XIV	
UBA-18702	13,261	60	16,730	15,540	−12.5	n/a	Land snail	*Helix melanostoma*	10,009	ARHC09S2-B	M	XIV	
UBA-18703	13,486	58	16,890	16,360	−11.8	n/a	Land snail	*Helix melanostoma*	10,009	ARHC09S3-A	M	XIV	
UBA-18704	12,439	57	15,000	14,140	−13.4	n/a	Land snail	*Helix melanostoma*	10,009	ARHC09S3-B	M	XIV	
UBA-18705	12,715	63	15,530	14,660	−10.1	n/a	Land snail	*Helix melanostoma*	10,009	ARHC09S5-A	M	XIV	
UBA-18706	12,613	57	15,220	14,260	−10.0	n/a	Land snail	*Helix melanostoma*	10,009	ARHC09S5-B	M	XIV	
UBA-18707	12,617	54	15,220	14,270	−10.6	n/a	Land snail	*Helix melanostoma*	10,009	ARHC09S7-A	M	XIV	
UBA-18708	12,696	54	15,500	14,630	−12.6	n/a	Land snail	*Helix melanostoma*	10,009	ARHC09S7-B	M	XIV	
UBA-18709	13,409	57	16,870	16,050	−11.2	n/a	Land snail	*Helix melanostoma*	10,009	ARHC09S7-C	M	XIV	
UBA-18710	13,096	57	16,450	15,220	−10.0	n/a	Land snail	*Helix melanostoma*	10,009	ARHC09S7-D	M	XIV	
UBA-18711	13,808	71	17,120	16,730	−7.9	n/a	Land snail	*Helix melanostoma*	10,009	ARHC09S7-E	M	XIV	
UBA-18712	13,915	60	17,200	16,780	−8.4	n/a	Land snail	*Helix melanostoma*	10,009	ARHC09S7-F	M	XIV	
UBA-18713	13,536	57	16,910	16,440	−13.6	n/a	Land snail	*Helix melanostoma*	10,011	ARHC11S1-A	M	XIV	
UBA-18714	13,269	56	16,740	15,560	−10.4	n/a	Land snail	*Helix melanostoma*	10,011	ARHC11S1-B	M	XIV	
UBA-18715	12,945	59	16,180	15,060	−11.6	n/a	Land snail	*Helix melanostoma*	10,011	ARHC11S1-C	M	XIV	
UBA-18716	13,333	57	16,830	15,640	−13.1	n/a	Land snail	*Helix melanostoma*	10,011	ARHC11S1-D	M	XIV	
UBA-18717	13,671	59	17,000	16,620	−11.3	n/a	Land snail	*Helix melanostoma*	10,011	ARHC11S1-E	M	XIV	
UBA-18718	13,852	61	17,140	16,760	−9.8	n/a	Land snail	*Helix melanostoma*	10,011	ARHC11S2-A	M	XIV	
UBA-18719	13,292	65	16,770	15,590	−9.9	n/a	Land snail	*Helix melanostoma*	10,011	ARHC11S2-B	M	XIV	
UBA-18720	13,545	89	16,940	16,370	−7.7	n/a	Land snail	*Helix melanostoma*	10,011	ARHC11S2-C	M	XIV	
UBA-18721	12,647	60	15,450	14,520	−15.8	n/a	Land snail	*Helix melanostoma*	10,011	ARHC11S2-D	M	XIV	
UBA-18722	12,644	55	15,420	14,530	−13.5	n/a	Land snail	*Helix melanostoma*	10,011	ARHC11S2-E	M	XIV	
UBA-18723	12,978	56	16,260	15,100	−9.3	n/a	Land snail	*Helix melanostoma*	10,011	ARHC11S2-F	M	XIV	
UBA-18724	12,610	58	15,210	14,250	−13.2	n/a	Land snail	*Helix melanostoma*	10,011	ARHC11S2-G	M	XIV	
OxA-21087	19,015	70	22,440	21,590	0.9	n/a	Marine shell	*Columbella rustica*		24,838		XIV–XV	McBurney Archive
OxA-21088	19,040	65	22,470	21,600	2.6	n/a	Marine shell	*Columbella rustica*		24,838		XIV–XV	McBurney Archive
OxA-21086	10,957	39	12,620	12,080	0.2	n/a	Marine shell	*Columbella rustica*		24,839		8–8.6′, Red II	McBurney Archive
OxA-21085	28,380	120	32,680	31,520	0.4	n/a	Marine shell	*Columbella rustica*		24,840		XX	McBurney Archive

The locations of the dating samples used in the Bayesian modelling are shown in Fig. 6 and SOM S1–S3. UT = Upper Trench; MT = Middle Trench.

with the Oranian/Capsian transition. The shells were scanned for post-depositional alteration using high-precision X-Ray diffraction (Douka et al., 2010a). No secondary calcite was identified and the samples were considered suitable for dating using the routine protocol of the ORAU, which involves phosphoric acid dissolution, and CO_2 purification prior to graphitization and AMS measurement (Brock et al., 2010). The three beads resulted in stratigraphically coherent dates (Table 1).

In the case of terrestrial molluscs, the dating program concentrated on *Helix melanostoma* because of the relatively constant pattern of fractionation found in in-progress Ph.D. research (see SOM 4: Radiocarbon (^{14}C) dating: terrestrial molluscs). Twenty-eight molluscs have been dated, all from Trench M (Contexts 10,006–10,011). Their ages closely correlate with a series of charred pine cones from the same contexts, the comparison of the two series allowing the calculation of the 'limestone effect' at the site (Goodfriend and Stipp, 1983).

All terrestrial ^{14}C measurements were calibrated using IntCal09, the most recent internationally agreed calibration curve available (Reimer et al., 2009). The four marine results were calibrated with Marine09, which incorporates a global marine reservoir correction of 400 ^{14}C years. In addition, a local Mediterranean reservoir correction of 58 ± 85 ^{14}C years was applied (Reimer and McCormac, 2002). The terrestrial gastropods were corrected for the 'limestone effect' by subtracting 410 ± 24 ^{14}C years prior to calibration (see SOM 4).

The five earliest radiocarbon dates (UBA-16129, UBA-16131–34 and OxA-22164), from Facies 5 and Facies 3 (Table 1 and Fig. 6) were obtained using the ABA pretreatment protocol, the method most widely used by all radiocarbon laboratories. However, it has been shown over the last few years that ABA does not efficiently decontaminate 'old' (>29–30 ka BP) charcoal samples when compared with a new more rigorous protocol (ABOx-SC: Bird et al., 1999): at almost all Palaeolithic sites where the latter has been applied, the results are older and more consistent both with the archaeological context and other independent markers, such as the Campanian Ignimbrite (CI) tephra (Douka et al., 2010b; Wood et al., 2012). The latter, ^{40}Ar/^{39}Ar dated at source to 39.28 ± 0.11 ka (error at 95.4% confidence interval) (De Vivo et al., 2001), has now been identified at the Haua Fteah (see below, Tephrochronology). The close association of the CI with UBA-1632 and UBA-16129, as well as with OxA-22164, suggests that the true age of these samples should be older, ~39.5 ka cal BP. When these samples were submitted for dating in 2008, the effect of ABOx-SC was not widely tested or appreciated.

The radiocarbon results in Facies 2 range from 27 ka to about 11 ka BP and agree well with the accepted age for Tephra T426 (see below, Tephrochronology), showing internal consistency with decreasing age moving up the stratigraphic column. The dates from Facies 1 also show good consistency, ranging from 12.3 ka BP to the Middle Holocene, and one reaches the historic period (OxA-18710). In some cases, however, where duplicate dates were produced from the same sample (e.g., sample HF 243), variations were observed. This is attributed to the nature of the sample and the bad preservation state: the charcoal fragments, for example, were almost always mixed with clayey sediment, which had to be physically and/or chemically removed during the pretreatment stage (see comments for each sample in Table 1). This opens the possibility that at least some of the samples were non-homogeneous, if not partially contaminated.

Tephrochronology

Contiguous 2 cm samples were taken through three overlapping vertical sampling columns on the west-facing section of the Middle Trench in order to investigate the presence of non-visible volcanic ash layers (cryptotephra) (Fig. 8). The sediment samples were processed in the laboratory following the methods described in Blockley et al. (2005), which aim to isolate volcanic glass from its host sediment using the physical properties of the tephra (density and grain size) (SOM 5: Tephrochronology). Initial investigations were carried out at a vertical sampling resolution of 5–10 cm respecting context boundaries (the interval was partly dependent upon the nature and thickness of the archaeological contexts). Concentrations of volcanic glass shards were calculated after counting from grain mounts under high-powered optical microscopy and are stated as the number of shards per gram of dry sediment (s/g). Where high concentrations of glass shards were

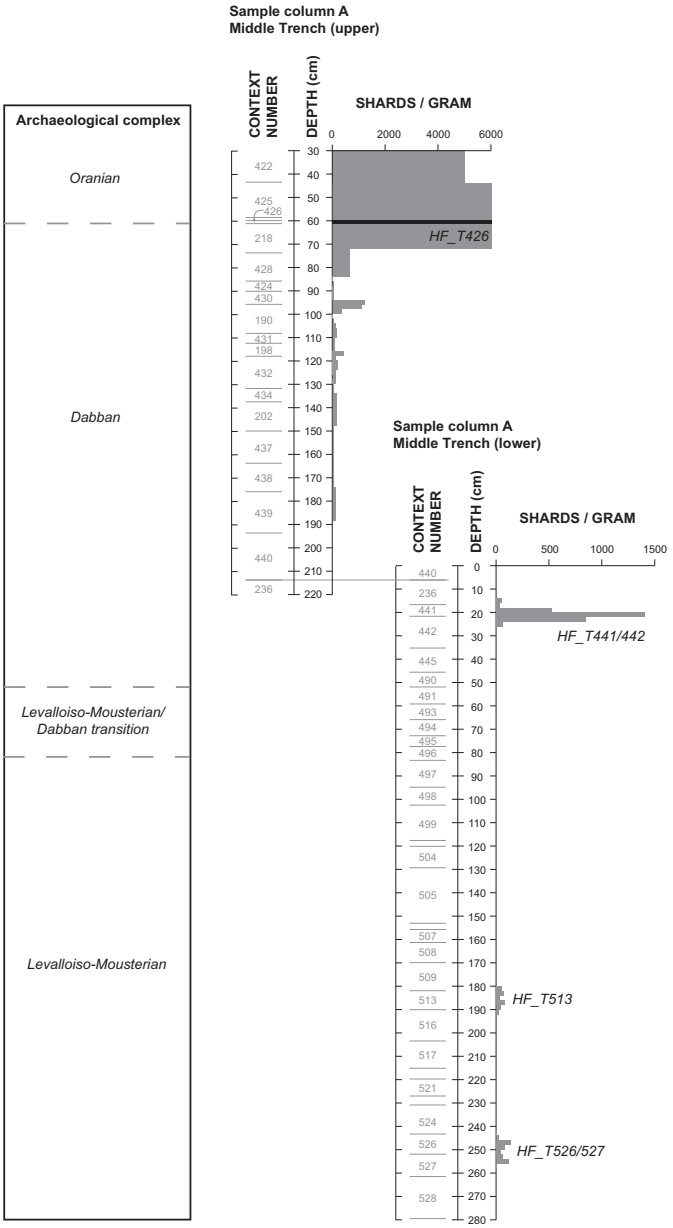

Figure 8. Tephra glass shard concentrations (shards/gram) for the upper and lower sample columns of the west-facing section of the Middle Trench (for location of sampling columns, see SOM Fig. S1). Approximate positions of archaeological complexes are noted in the left hand column. Context numbers refer to the CPP excavations. Microscopic inspection and chemical analysis confirm that the high tephra concentrations in the uppermost 72 cm represent remobilisation of tephra glass shards from the HF-T426 tephra layer (context 426), as do the fluctuating concentrations below it, an example of the bioturbation affecting the Haua Fteah sediments.

located, these samples were re-visited at 2 cm resolution to pinpoint more precisely the stratigraphic position of the tephra horizon. A short section of the north-facing Trench M was also investigated at lower resolution. Tephra and standard results are presented in SOM Tables S2 and S3. Four tephra layers were located in the Middle Trench west-facing sample columns, of which the first three have been correlated to dated eruption events.

HF_T426 The ~1 cm thick Context 426, at 60 cm depth in the sampling column, has been confirmed as a visible tephra layer that can be traced around the walls of the Middle Trench, occurring as Context 10,008 in Trench M (Fig. 6). Macroscopically the layer is a very fine-grained, grey, ashy horizon, which shows clear horizontal continuity (SOM Fig. S4). Under microscopic inspection, the layer is seen to be composed almost entirely of volcanic glass shards (<0.5% detrital grains content). These shards show a wide variety of morphologies, texture and colour. The shards generally show a low angularity and range from clear to light brown irregular shards with both open elongate and closed circular vesicles, to more blocky light brown shards with high microcryst content. Microcrysts are present in around 25% of the shards, either as isolated tabular crystals or in randomly oriented clusters. Shard sizes range from 30 to 250 μm on the longest axis. The homogeneous trachytic glass composition of HF_T426 correlates to the most recent Plinian caldera-forming event from Mount Etna in Sicily, known as the Biancavilla Ignimbrite (Coltelli et al., 2000; Albert et al., 2013; Fig. 8b). A radiocarbon age estimate of 14,180 ± 260 BP or 17,920–16,810 cal BP (Kieffer, 1979; calibrated using IntCal09: Reimer et al., 2009) is reported from an in situ carbonized tree beneath the Biancavilla flow units at Vallone San Filippo.

HF_T441/442 A clearly defined rise in tephra shard concentrations was located at 18–24 cm depth within sampling column A (lower) (Fig. 8). The peak concentration of ~1400 s/g is centred at 20–22 cm, which lies at the contact between Contexts 441 and 442, a layer not visible macroscopically within the stratigraphy. The tephra shards in HF_T441/442 are colourless with platy to curvilinear form, often displaying fluted structures from the elongation of vesicles. Grain sizes (measurement of the longest axis) are <160 μm. Glass shards from T441/442 show a homogeneous phono-trachytic major and minor element composition (Fig. 9c). The Campi Flegrei has produced multiple Plinian and sub-Plinian eruptions over the last >60 ka (Wulf et al., 2004). The largest of these was the Campanian Ignimbrite (CI), a caldera-forming event that erupted 250–300 km^3 of magma (Costa et al., 2012). Detailed glass analysis from the main fall and flow units sampled close to the eruptive centre (more complete representations of tephra chemical composition than distal ashes: Albert et al., 2012) has recently been carried out by Tomlinson et al. (2012a). The compositional data from HF_T441/442 show a good match to this proximal record (Lowe et al., 2012; Fig. 9c). Major, minor and trace element concentrations separate

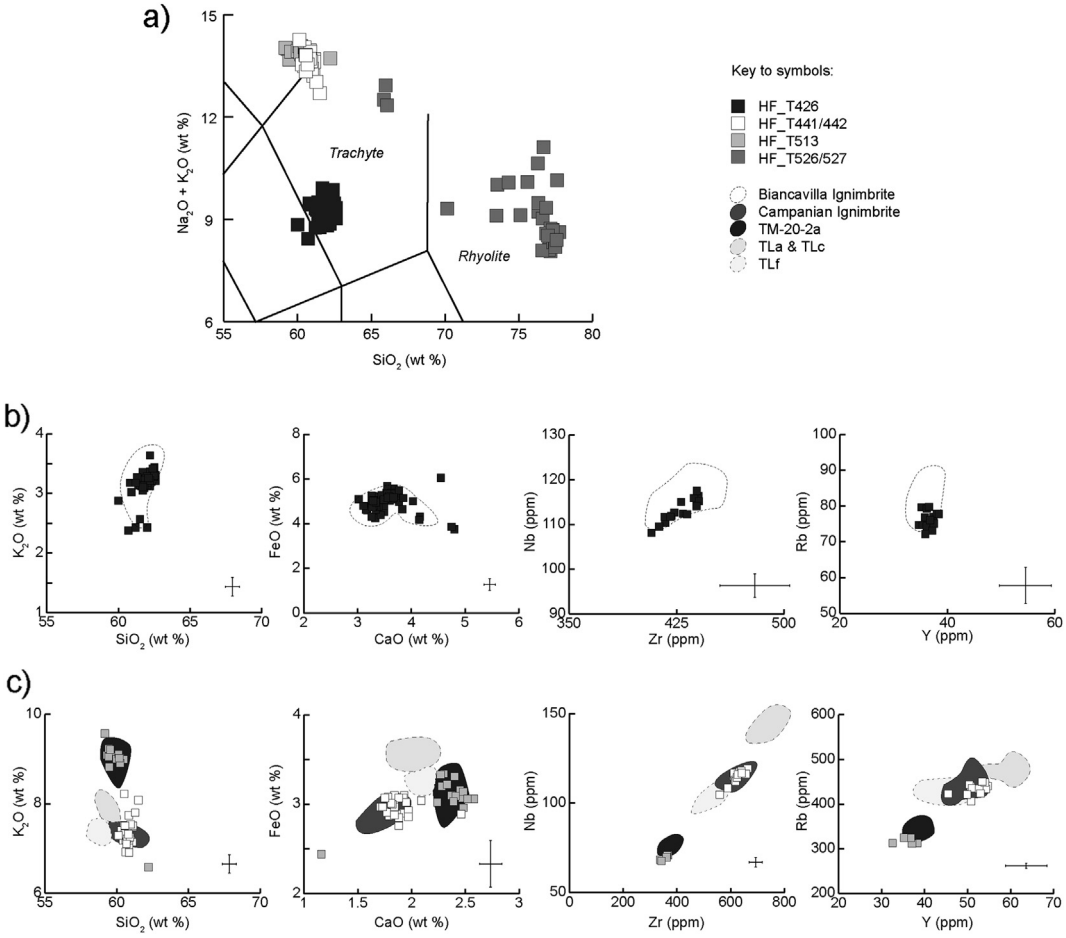

Figure 9. Glass composition of the Haua Fteah tephra layers (WDS-EPMA and LA–ICP–MS) and comparative reference data: (a) total-alkali-silica plot of tephra layers from the Haua Fteah; (b) HF_T426 compared to glass compositional envelope from Acireale proximal fallout deposit of the Biancavilla tephra (Albert et al., 2013); (c) HF_T441/442 and HF_T513 plotted alongside glass compositional envelopes from proximal outcrops of the CI main flow and fall units and three proximally described pre-CI Campi Flegrei events TLa, TLc and TLf (data from Tomlinson et al., 2012a) and data from tephra layer TM-20-2a in Lago Grande di Monticchio. Error bars in bottom right corner of each plot indicate approximate two standard deviation uncertainty ranges for data produced within this study, based upon the reproducibility of secondary standard analyses run alongside the tephra data.

the CI from the largest of a number of precursor events (TLa, TLc and TLf: Orsi et al., 1996; Pabst et al., 2008; Tomlinson et al., 2012a) and confirm that HF_T441/442 can confidently be assigned to the main explosive phase of the CI eruption. As previously mentioned, the CI has been $^{40}Ar/^{39}Ar$ dated to 39.28 ± 0.11 ka BP (De Vivo et al., 2001).

HF_T513 A third tephra layer was located within Context 513, at 180–192 cm depth in Middle Trench sample column A (lower) (Fig. 8). The maximum shard concentration was 86 s/g. Morphologically, the tephra shards appear similar to those in HF_T441/442, although grain sizes (measurement of the longest axis) are limited to <80 μm. Major and minor element analysis of T513 describes a phonolitic composition, with only one compositional outlier sitting within the trachytic field of a total alkali silica diagram (Fig. 9c). The broad compositional similarity of HF_T513 with HF_T441/442 suggests that they are from the same Campi Flegrei source area, but, as can be seen in the major and trace element bi-plots, the two eruptions are compositionally distinct. Several 'Pre-CI' tephra layers have been described from outcrops within the Campi Flegrei (e.g., TLa, TLc and TLf: Orsi et al., 1996; Pabst et al., 2008; Tomlinson et al., 2012a), at sites across the Campanian Plain (e.g., SA3-a: Di Vito et al., 2008) and within the high resolution tephrostratigraphic record of Lago Grande di Monticchio (e.g., TM-20-2a and >8 other layers: Wulf et al., 2004). Based upon major, minor and trace elements compositions, the closest match for HF_T513 is to glass composition data on the TM-20-2a tephra layer from Lago Grande di Monticchio (Wulf et al., 2007; Fig. 9c). The latter, found at a depth of 43.5 m and 6.0 mm thick, was most likely generated by a much lower magnitude eruption than, for example, the CI (~260.0 mm). TM-20-2a has a varve age of 68,620 ± 2060 calendar years (ca. 3% varve counting error).

HF_T526/527 Tephra shards were found throughout Contexts 526 and 527 in concentrations of <141 s/g, and in trace concentrations (<5 s/g), reaching into the base of Context 524 and the upper part of Context 528 (Fig. 8). The distribution is variable, concentrated mainly at 248–258 cm depth, at the boundary between the two contexts. Shard morphologies show a range of platy, rather featureless, curvilinear forms, to elongate fluted and angular shards with open vesicles. All shards are colourless and have maximum long axis of ~70 μm. Sample HF T526/527 within WDS-EPMA had a variable chemical composition, being comprised of at least two rhyolitic populations and a smaller number of shards of trachytic composition (Fig. 9c). This variability indicates a mixed population of tephra from multiple volcanic events. These events may have occurred closely spaced in time, or their proximity may result from reduced sedimentation rates and syn-depositional reworking, which would cause them to be spread out and mixed within the stratigraphy. In the pre-CI Mediterranean volcanic record, a small number of explosive eruptions are believed to have generated widespread rhyolitic tephra layers. These include eruptions from Nisyros Island in the Hellenic Arc (Volentik et al., 2005; Tomlinson et al., 2012b) and numerous eruptions from rhyolitic centres in the Central Anatolian Province such as Acigöl and Hasan Dagi (Deniel et al., 1998; Kuzucuoglu et al., 1998; Mouralis et al., 2002). However, all of these events are poorly dated, little is known about the distal dispersal of their tephra, and where single-grain glass chemistry is available it does not show a match for HF_T526/527, which at present, therefore, remains uncorrelated.

OSL dating

Twelve samples for OSL dating were collected at semi-regular intervals (~every 30–50 cm) from the top to the bottom of the south face (north-facing section) of the Middle Trench (Figs. 5 and 6). The samples were measured and analysed in the OSL dating laboratory at the University of Wollongong (UOW), Australia. One duplicate sample (HF10) was measured in the OSL dating laboratory at Royal Holloway, University of London, UK (Russell and Armitage, 2012). The sample names and associated sample contexts are listed in Table 2. Full details of sample collection, preparation and measurements are provided in SOM 6: Optically stimulated luminescence dating.

The equivalent dose (D_e) is a measure of the radiation energy absorbed by a grain during the period of burial. We measured D_e values in two ways, owing to the paucity of grains in our preferred grain size fraction (180–212 μm in diameter). We first measured multi-grain aliquots of each sample, in which each aliquot consisted of either ~15 grains of 60–90 μm in diameter, or ~8 grains of 90–125 μm in diameter. Because the multi-grain aliquots each represents the average of many grains, it is not possible to decipher from these measurements alone what the D_e distributions may mean with regards to grain behaviour and burial history. This can only be achieved by measurement of individual grains (e.g., Jacobs and Roberts, 2007). Therefore, in this study, we also measured individually the few grains recovered of 90–125 μm and 125–212 μm in diameter. This allowed us to test whether we are obtaining accurate estimates of D_e using small multi-grain aliquots and how these values could be combined to obtain a final estimate of D_e for age calculation.

Of the 8200 multi-grain aliquots measured, 3272 aliquots (39.9% of the total number measured) were used for final D_e determination. Reasons for rejecting multi-grain aliquots are provided in SOM Table S4. On average, most aliquots were rejected due to poor recycling ratios. Those that were accepted were typical of aliquots dominated by the fast-component (SOM Fig. S8a). The D_e values for the accepted aliquots for each sample are displayed as radial plots in the left-hand column of SOM Fig. S10 and a representative example is provided in Fig. 10. In such plots, the most precise estimates fall to the right and the least precise to the left. If these independent estimates are consistent with statistical expectations, then 95% of the points should scatter within a band of width ±2 units projecting from the left-hand ('standardised estimate') axis to any chosen D_e value on the right-hand, radial axis. The radial plots, thus, provide simultaneous information about the spread, precision and statistical consistency of the D_e values (Galbraith, 1988, 1990).

It is immediately apparent from these plots that, for each of the samples, the D_e estimates are spread too widely to fall within any single band of ±2 units. This is also reflected in the D_e overdispersion values (Table 2), which range from 15 ± 1% (HF1) to 30 ± 4% (HF9), and are greater than the 7% overdispersion obtained for sample HF7 under controlled laboratory conditions in a dose recovery test. However, all of the radial plots show that the vast majority of the D_e values are spread symmetrically around a common value. Such patterns are typical of samples that have been well-bleached prior to deposition and that have remained undisturbed since burial. There are, however, three interesting characteristics of note: a few samples show very distinct hard base-lines in their distributions (e.g., HF3), several samples show evidence of significant low outlier D_e values (e.g., HF7 and HF9), and some of the samples (e.g., HF10 and HF11) almost appear to consist of more than one population of D_e values.

Of the 6200 individual grains measured, only 780 grains (12.6%) were used for final D_e determination. Reasons for rejecting individual grains are provided in SOM Table S4. On average, most grains were rejected because they were too dim following a laboratory dose (T_N signal < 3xBG). The D_e values for the accepted grains in each sample are displayed as radial plots in the right-hand column of SOM Fig. S10 and a representative example is provided in Fig. 10.

Table 2
Dose rate data, D_e values and OSL ages for multi-grain aliquots and single grains of 12 sediment samples from the Haua Fteah.

Sample name	Sample context	Grain size (μm)	Water content (%)	Dose rate (Gy/ka)				Number of aliquots or grains	Over-dispersion (%)	D_e value (Gy)	Age[a] (ka)
				Beta	Gamma	Cosmic	Total				
HF1	180	60–90	2.7	1.07 ± 0.06	0.22 ± 0.01	0.045	1.37 ± 0.07	593/1000 (MG)	15 ± 1	25.1 ± 0.2	18.4 ± 1.0
		180–212		1.00 ± 0.06			1.29 ± 0.07	53/100 (SG)	24 ± 4	26.0 ± 1.1	**19.3 ± 1.4**
HF2	185–188/189	60–90	11.1	1.61 ± 0.09	0.47 ± 0.02	0.045	2.15 ± 0.13	510/900 (MG)	18 ± 1	43.2 ± 0.4	20.1 ± 1.3
		90–125		1.58 ± 0.09			2.12 ± 0.13	52/200 (SG)	25 ± 4	38.7 ± 1.5	**18.3 ± 1.4**
HF3	201	60–90	24.8	1.06 ± 0.07	0.48 ± 0.02	0.044	1.61 ± 0.13	534/1000 (MG)	18 ± 1	52.0 ± 0.5	32.4 ± 2.8
		90–125		1.04 ± 0.07			1.59 ± 0.13	24/200 (SG)	65 ± 11 (25 ± 6)	50.6 ± 3.4	**31.9 ± 3.5**
HF4	235,439,444	90–125	30.7	1.78 ± 0.13	0.71 ± 0.04	0.042	2.73 ± 0.21	354/500 (MG)	24 ± 1	97.7 ± 1.6	38.2 ± 3.7
HF5	453	90–125	36.6	1.11 ± 0.08	0.65 ± 0.03	0.042	1.84 ± 0.18	129/200 (SG)	24 ± 2	86.8 ± 2.3	**47.2 ± 4.9**
HF6	498	90–125	37.0	1.46 ± 0.11	0.77 ± 0.04	0.041	2.30 ± 0.23	55/400 (MG)	29 ± 5	74.9 ± 4.0	32.6 ± 3.8
		180–212		1.38 ± 0.11			2.22 ± 0.22	27/500 (SG)	168 ± 24 (26 ± 6)	106.4 ± 7.7	**47.9 ± 6.0**
HF7	503/504	90–125	33.8	1.34 ± 0.10	0.78 ± 0.04	0.040	2.18 ± 0.21	190/500 (MG)	24 ± 2	104.8 ± 2.8	48.0 ± 4.9
								57/1000 (SG)	97 ± 10 (30 ± 4)	105.5 ± 5.4	**48.3 ± 5.3**
HF8	513	90–125	29.2	1.37 ± 0.10	0.70 ± 0.04	0.039	2.01 ± 0.19	175/500 (MG)	21 ± 2	106.4 ± 2.5	49.8 ± 4.7
		125–180		1.30 ± 0.10			2.06 ± 0.19	120/1000 (SG)	60 ± 5 (20 ± 3)	95.0 ± 2.7	**46.2 ± 4.5**
HF9	536/537/562	90–125	22.0	0.72 ± 0.05	0.56 ± 0.03	0.038	1.35 ± 0.11	82/1000 (MG)	30 ± 4	89.2 ± 3.2	66.0 ± 5.8
		180–212		0.68 ± 0.05			1.31 ± 0.10	87/800 (SG)	49 ± 5 (24 ± 4)	91.5 ± 3.6	**69.7 ± 6.3**
HF10	524	60–90	34.6	1.36 ± 0.10	0.72 ± 0.04	0.038	2.15 ± 0.21	373/900 (MG)	26 ± 2	130.8 ± 2.5	60.9 ± 6.1
		180–212		1.26 ± 0.10			2.05 ± 0.20	112/2000 (SG)	19 ± 4	130.7 ± 3.7	**63.7 ± 6.6**
HF11	528	90–125	28.4	1.12 ± 0.08	0.72 ± 0.04	0.037	1.91 ± 0.17	405/1000 (MG)	26 ± 1	125.8 ± 1.7	65.8 ± 6.0
		125–212		1.06 ± 0.08			1.85 ± 0.16	81/1000 (SG)	25 ± 4	131.1 ± 5.2	**70.9 ± 7.0**
HF12	525/565	180–212	25.6	1.03 ± 0.07	0.72 ± 0.04	0.036	1.81 ± 0.15	33/900 (SG)	24 ± 6	130.3 ± 7.9	**71.9 ± 7.6**

We consider the single-grain OSL chronology to be more reliable for our samples and those ages are highlighted in bold; see text for discussion.
[a] Standard error includes all random and systematic uncertainties; see text for discussion.

Like the multi-grain aliquots, the single grain D_e distributions are also spread more widely than can be explained by measurement uncertainties alone. The single-grain D_e distributions are over-dispersed by between 19 ± 4% (HF10) and 168 ± 24% (HF6) (Table 2). The lower end of this range is typical of samples measured from around the world that are considered to be well-bleached prior to deposition, and that remained undisturbed since burial (Olley et al., 2004; Thomsen et al., 2005, 2007; Jacobs et al., 2006; Arnold and Roberts, 2009; Galbraith and Roberts, 2012), but the upper end suggests significant contamination. However, the data cannot be interpreted without looking at the D_e distribution patterns when displayed as radial plots (SOM Fig. S6). From these it is evident that the large overdispersion for some of the samples is due to the presence of only a few precisely known grains that are 'modern' in age and that form a discrete D_e population (e.g., SOM Fig. S10: HF6). Note that in some samples there are also a number of grains with smaller-than-average D_e values, but that are not consistent with zero. Such grains are considered part of the D_e distribution of those samples (e.g., SOM Fig. S11: HF9). We have also noted in SOM Table S5 that in many of these samples, there were always a few grains that were rejected on the basis of them being 'modern' (i.e., they have precise dose response curves, but no natural signal). These D_e values are not shown on the radial plots, since negative and zero D_e values cannot easily be plotted on such graphs (e.g., Arnold et al., 2009). So, in actual fact, the over-dispersion values for these samples will be even larger. We are not sure how to interpret the results for such grains: they might simply be light-exposed grains that were not removed properly when sample preparation commenced, or they could be grains belonging to the 1950s backfill that were incorporated through bioturbation of sediments by e.g., mole rats, observed as burrows in the field (see section on 'The sedimentary sequence'). This may also explain the very young ^{14}C ages that were obtained for five of the charcoal samples (Table 1). If these grains are removed from the D_e

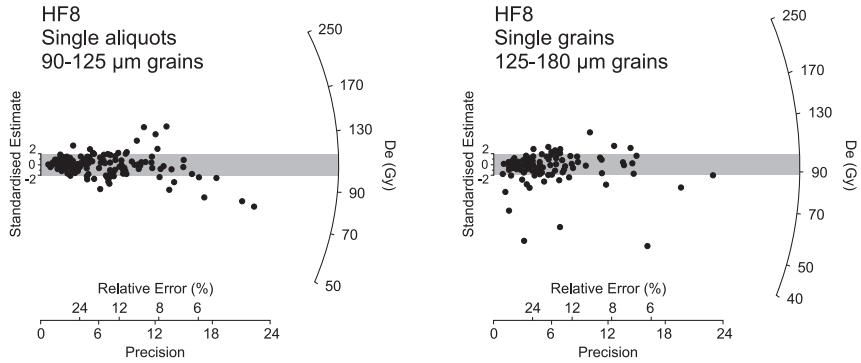

Figure 10. Representative radial plots of multi-grain aliquot and single-grain D_e distributions for OSL samples from the Haua Fteah. The plots shown here are for sample HF8; plots for all samples are provided in SOM 6. The OSL age for this sample was estimated using the central age model (CAM); the grey band is centred on the CAM weighted mean D_e value in each plot.

Table 3
ESR dating of tooth samples (all bovid, mainly *Ammotragus* sp.) from the Haua Fteah; see text and SOM 7 for discussion; dose-rate conversion factors after Guerin et al. (2011).

Lab number	CPP sample number	Location	Context	D_e (Gy)	U(EN) (ppm)	U(DE) (ppm)	Thickness[a] (μm)	U(SED) (ppm)	Th(SED) (ppm)	K(SED) (ppm)	Gamma(SED) DR[b] (μGy/a)	Beta(SED) DR[b] (μGy/a)	U-234/U-238	Th-230/U-238	U-series age (ka)	US-ESR calculations							CSUS-ESR
																p-Value	Internal (EN) DR (μGy/a)	Beta (DE) DR (μGy/a)	Total DR (μGy/a)	Age (ka)	+Error (ka)	−Error (ka)	Age (ka)
2564	831	Middle Trench	422	17.6 ± 1.0	0.22	17.6	950	2.37	7.45	13,200	1003 ± 80	183 ± 13	1.09 ± 0.01	0.071 ± 0.014	7.3	−0.12 ± 0.46	15 ± 5	76 ± 26	1277 ± 85	13.7	1.3	1.2	13 ± 1
2565	832	Middle Trench	425	31.9 ± 1.6	0.14	16.7	700	2.09	9.34	15,300	1003 ± 80	264 ± 29	1.08 ± 0.01	0.081 ± 0.013	8.5	0.74 ± 0.57	6 ± 2	64 ± 20	1337 ± 85	23.8	2.2	1.9	23 ± 2
2566	721	Middle Trench	249	18.4 ± 1.4	0.06	6.9	850	2.17	10.67	18,000	1003 ± 80	257 ± 27	1.04 ± 0.01	0.042 ± 0.023	4.5	1.18 ± 1.23	2 ± 1	19 ± 13	1281 ± 85	14.3	1.5	1.4	14 ± 1
2568	723	Middle Trench	177	17.3 ± 1.9	0.03	3.3	1600	1.91	9.64	18,600	1003 ± 80	137 ± 13	1.05 ± 0.01	0.030 ± 0.050	3.2	2.65 ± 1.89	0 ± 0	3 ± 2	1143 ± 85	15.1	2.0	1.9	15 ± 2
2569	776	Middle Trench	190	17.9 ± 1.0	0.14	7.7	1100	1.77	6.47	11,000	1003 ± 80	130 ± 14	1.07 ± 0.01	0.035 ± 0.024	3.6	2.22 ± 1.71	4 ± 4	5 ± 4	1142 ± 85	15.6	1.5	1.3	15 ± 1
2570	778	Middle Trench	217	17.5 ± 1.1	0.47	15.4	1350	2.44	8.62	13,700	1003 ± 80	137 ± 14	1.08 ± 0.01	0.082 ± 0.013	8.6	−0.38 ± 0.32	40 ± 12	58 ± 17	1238 ± 85	14.1	1.5	1.3	14 ± 1
2571	882	Middle Trench	240	22.8 ± 1.1	1.04	18.9	1300	1.77	8.44	15,600	1003 ± 80	145 ± 14	1.10 ± 0.01	0.095 ± 0.012	9.9	−0.24 ± 0.30	85 ± 24	69 ± 17	1302 ± 86	17.5	1.7	1.5	17 ± 1
2573	933	Middle Trench	422	22.3 ± 1.5	0.26	20.7	800	2.16	8.17	15,000	1003 ± 80	230 ± 24	1.08 ± 0.01	0.060 ± 0.010	6.2	0.65 ± 0.53	12 ± 3	73 ± 22	1318 ± 86	16.9	1.7	1.6	16 ± 1

Lab number	CPP sample number	Location	Context	D_e (Gy)	U(EN) (ppm)	U(DE) (ppm)	Thickness[a] (μm)	U(SED) (ppm)	Th(SED) (ppm)	K(SED) (ppm)	Gamma(SED) DR[b] (μGy/a)	Beta(SED) DR[b] (μGy/a)	U-234/U-238[c]	EU-ESR calculations				LU-ESR calculations			
														Internal (EN) DR (μGy/a)	Beta (DE) DR (μGy/a)	Total DR (μGy/a)	Age (ka)	Internal (EN) DR (μGy/a)	Beta (DE) DR (μGy/a)	Total DR	Age (ka)
2697	3013	Trench M	10,001	9.9 ± 0.4	0.11	4.5	1000	2.03	10.59	19,700	920 ± 115	232 ± 24	1.074 ± 0.020	14 ± 3	35 ± 3	1201 ± 117	8.2 ± 0.8	7 ± 1	17 ± 1	1176 ± 117	8.4 ± 0.9
2698	3021	Trench M	10,001	9.0 ± 1.2	0.26	6.3	900	2.06	9.45	17,700	920 ± 115	235 ± 25	1.074 ± 0.020	33 ± 5	54 ± 4	1242 ± 117	7.2 ± 1.1	16 ± 2	26 ± 2	1197 ± 117	7.5 ± 1.2
2699	3031	Trench M	10,001	10.5 ± 0.6	0.11	6.0	1150	1.81	6.37	11,900	920 ± 115	131 ± 13	1.074 ± 0.020	15 ± 2	42 ± 3	1108 ± 115	9.4 ± 1.1	7 ± 1	20 ± 1	1078 ± 115	9.7 ± 1.1
2700	3045	Trench M	10,001	9.7 ± 0.9	0.05	3.6	1500	1.89	7.24	13,400	920 ± 115	112 ± 12	1.074 ± 0.020	6 ± 3	20 ± 1	1058 ± 115	9.1 ± 1.3	3 ± 1	9 ± 1	1044 ± 115	9.2 ± 1.3
2701	3066	Trench M	10,001	9.5 ± 0.5	0.29	4.9	1550	1.77	6.04	12,100	920 ± 115	97 ± 9	1.074 ± 0.020	40 ± 5	26 ± 1	1083 ± 115	8.7 ± 1.0	19 ± 2	13 ± 1	1049 ± 115	9.0 ± 1.0
2702	3069	Trench M	10,001	9.7 ± 0.7	0.17	4.2	1100	2.27	5.62	11,500	920 ± 115	139 ± 14	1.074 ± 0.020	23 ± 2	30 ± 2	1112 ± 115	8.7 ± 1.1	11 ± 1	15 ± 1	1085 ± 116	8.9 ± 1.1
2703	3074	Trench M	10,004	7.6 ± 0.8	0.33	5.0	1050	2.44	5.71	7900	920 ± 115	120 ± 13	1.074 ± 0.020	43 ± 4	37 ± 3	1120 ± 115	6.7 ± 1.0	21 ± 3	18 ± 1	1079 ± 115	7.0 ± 1.0
2704	3076	Trench M	10,005	9.6 ± 0.5	0.15	1.9	1150	1.90	8.23	17,800	920 ± 115	180 ± 18	1.074 ± 0.020	20 ± 2	13 ± 1	1133 ± 116	8.3 ± 0.9	9 ± 2	6 ± 1	1115 ± 116	8.5 ± 0.9
2705	3095	Trench M	10,005	9.8 ± 1.0	0.18	6.1	900	2.22	7.09	15,500	920 ± 115	210 ± 23	1.074 ± 0.020	23 ± 4	52 ± 3	1205 ± 117	8.1 ± 1.1	11 ± 1	25 ± 2	1166 ± 117	8.4 ± 1.2
2706	3101	Trench M	10,005	10.6 ± 2.2	0.20	5.5	850	1.56	5.93	11,300	920 ± 115	162 ± 17	1.074 ± 0.020	26 ± 4	50 ± 4	1158 ± 116	9.1 ± 2.1	12 ± 2	24 ± 2	1118 ± 116	9.4 ± 2.2
2707	3145	Trench M	10,001	7.4 ± 0.5	0.13	2.8	1400	1.60	7.43	13,700	920 ± 125	118 ± 12	1.074 ± 0.020	17 ± 3	16 ± 1	1071 ± 115	6.9 ± 0.8	8 ± 1	8 ± 1	1054 ± 115	7.0 ± 0.9

Notes: D_e: Equivalent Dose; DR: Dose Rate; EN: Enamel; DE: Dentine; SED: Sediment; US-ESR: Combined U-series/ESR dating (Grün et al., 1988); CSUS-ESR: Closed system U-series – ESR dating (Grün, 2000); EU: Early U uptake; LU: Linear U uptake.
Age calculations with ESR data (Grün, 2009b).
Detection limits: U: 0.01 ppm; Th: 0.03 ppm; K: 500 ppm.
Alpha efficiency: 0.13 ± 0.02 (Grün and Katzenberger-Apel, 1994).
[a] 50 μm removed from each side; 25 μm uncertainty in each measurement.
[b] Water: 10 ± 5%.
[c] Average from first data set.

distributions, then the overdispersion values for the different samples (indicated in brackets in Table 2) range between 19 ± 1% (HF10) and 40 ± 4% (HF9), similar to the range observed for the multi-grain aliquot measurements.

The random incorporation of these 'modern' grains into a multi-grain aliquot can also explain all three of the patterns discussed above for the multi-grain aliquots. 'Modern' grains represent between 2.3% (HF9) and 38.9% (HF6) of the measured grains in the samples where they were observed. How their incorporation into the multi-grain aliquots affected the final D_e value will partly depend on the proportion of modern grains measured for each sample: the higher the proportion, the more likely it will be to get an underestimate of D_e from multi-grain aliquots. When these 'modern' grains are omitted from the D_e distributions, the single-grain D_e distributions can be best explained as having been well-bleached prior to deposition and undisturbed since burial.

We used the central age model (CAM) of Galbraith et al. (1999) to combine the individual multi-grain and single-grain D_e values meaningfully in order to obtain the most accurate estimate of D_e for age calculation. For the single-grain distributions, we first removed the 'modern' grains before applying the CAM. The smaller-than-average D_e values, other than those that are 'modern', were not removed; their inclusion would lead to a larger uncertainty on the CAM D_e value, but they do not appear to skew the weighted mean value significantly. The CAM model assumes that the D_e values for all grains/aliquots are centred on some average value of D_e (similar to the median) and the estimated standard error takes account of any overdispersion. Information about the number of grains measured and used, the grain size, overdispersion values calculated and the final $D_e \pm 1\sigma$ value for each sample is presented in Table 2 for the multi-grain and single-grain measurements.

The environmental dose rates (the rate of supply of ionising radiation to the grains over the burial period) mostly vary over a narrow range between 1.6 and 2.3 Gy/ka, and there is no obvious pattern of variation with depth (Table 2). There is one conspicuously higher value of 2.73 Gy/ka for HF4. There are also two samples (HF1 and HF9) with lower dose rates of ~1.30–1.37 Gy/ka, respectively. Sample HF1 was collected from a loose snail-shell rich layer, whereas sample HF9 was collected from a yellow baked layer underneath some ashy material. HF1 also had much lower moisture content than any of the underlying samples, which contained a much higher proportion of silts and clays.

The D_e and dose rate information is presented in Table 2, together with the OSL ages for all samples. The OSL ages for the twelve samples are in correct stratigraphic order for both the small multi-grain aliquots and the single grains. Both aliquots and grains produce statistically comparable ages where comparisons are available for eight samples, with the notable exception of HF6. This sample was unusual in that 38.9% of the individual grains measured were 'modern' (SOM Table S4), and while these grains could be identified and removed from the single grain data set, they appeared to have contaminated a significant fraction of the multi-grain aliquots of this sample. For this reason, amongst others, we consider the single-grain OSL chronology to be more reliable for our samples and those ages are highlighted in bold in Table 2. The ages range from ca. 19 ka at the top of the Middle Trench (HF1) to ca. 70 ka at the base (HF12). The four lowermost samples (HF9–12) date to between 70 and 65 ka, and the overlying four samples (HF5–8) all cluster closely at ca. 47–48 ka. HF4 and HF3 gave ages of 38 ± 4 ka and 32 ± 4 ka, respectively. The uppermost two samples (HF2 and HF1) gave statistically consistent results of ca. 18–19 ka. Overall, therefore, there is good internal stratigraphic coherence amongst all of the OSL ages, whilst they also confirm the very variable rates of sedimentation indicated by the sedimentological and stratigraphic studies discussed above.

There are, in general, good correspondences between the OSL ages, ^{14}C ages and ages of the tephra horizons, apart from the apparent mismatch between the OSL age for HF8 of 46 ± 5 ka and the age of the tephra (T513) in the same context of 68.6 ± 2.1 ka. We observed at the time of sampling that sample HF8 was collected from hearth-ash mixed in with sediment and that the sediments were likely post-dating the hearth-like layer. As noted above, the underlying sample, HF9, with an OSL age (70 ± 6 ka) consistent with the tephra age, was collected immediately underneath this hearth-like layer in a yellowish baked sediment layer. Thus, HF8 sediments may have been incorporated at ca. 46 ka into the underlying layers in which the tephra shards were found. This also agrees with the sedimentological observation that the top of Facies 4, from which HF8 was collected, represents a heavily weathered anthropogenic burning event, suggestive of a relatively long surface exposure. In other words, if the sediments associated with this burning event represent the last time that the surface was exposed to sunlight, and the assumption is that that surface represents a significant hiatus in sediment deposition, then one would expect the OSL age to be much younger than the in situ and underlying tephra, and more similar to the ages of the start of Facies 3, which essentially buried the surface sediments exposed at the top of Facies 4. The OSL age for the base of Facies 3 is indeed consistent with that obtained for HF8 at the top of Facies 4.

None of the OSL samples is stratigraphically directly comparable with the CI tephra (T441/442), but two of the OSL ages bracket this layer (HF4 and HF5). Sample HF5, located ~30 cm below T441/442 and dated to 47 ± 5 ka, is older than TT441/442. Sample HF4, located ~20 cm above T441/442, unfortunately did not yield sufficient grains >125 μm in diameter, but the multi-grain aliquot age of 38 ± 4 ka corresponds closely with the $^{40}Ar/^{39}Ar$ age for the CI tephra of 39.28 ± 0.11 ka (De Vivo et al., 2001).

The uppermost and macroscopically visible tephra layer (T426) was identified along the east face (west-facing section) of the Middle Trench and corresponds most closely with OSL sample HF2 located immediately above it, which gave an age of 18 ± 1 ka. This is statistically consistent with the age assigned to the tephra of 16.8–17.9 ka cal BP at the 95% confidence interval, and with a range of consistent ^{14}C ages. The uppermost OSL sample HF1 that gave an age of 19 ± 1 ka appears, however, to be systematically too old by 4–5 ka when compared to ^{14}C ages from similar or slightly deeper contexts (e.g., OxA-19029, OxA-19185, OxA-19186, OxA-19187 and OxA-19188).

An inter-laboratory comparison of sample HF10, from which a duplicate tube was dated at Royal Holloway, University of London (Russell and Armitage, 2012), is discussed in the SOM.

ESR dating

Animal teeth were collected from the cleaned faces of the Middle Trench, especially from the north-facing section, and sent for ESR dating to the Australian National University (Canberra) in two batches (Table 3: Sample numbers 2564–2573 and 2697–2707). Sample preparation and ESR measurements followed the routine procedures of the ANU ESR laboratory (see SOM 7. ESR dating). Because of relatively low U-concentrations and strong U-series disequilibria, the internal enamel and dentine dose rates are very small. The differences in the age results using the p-value system and the closed system U-series/ESR model are within rounding errors (Grün, 2000). Because of the insignificant dose rate contributions of uranium in the dental tissues, the second set was not further analysed for U-series isotopes. The differences between the parametric early and linear U-uptake models (EU and LU) are no more than 300 years. This is

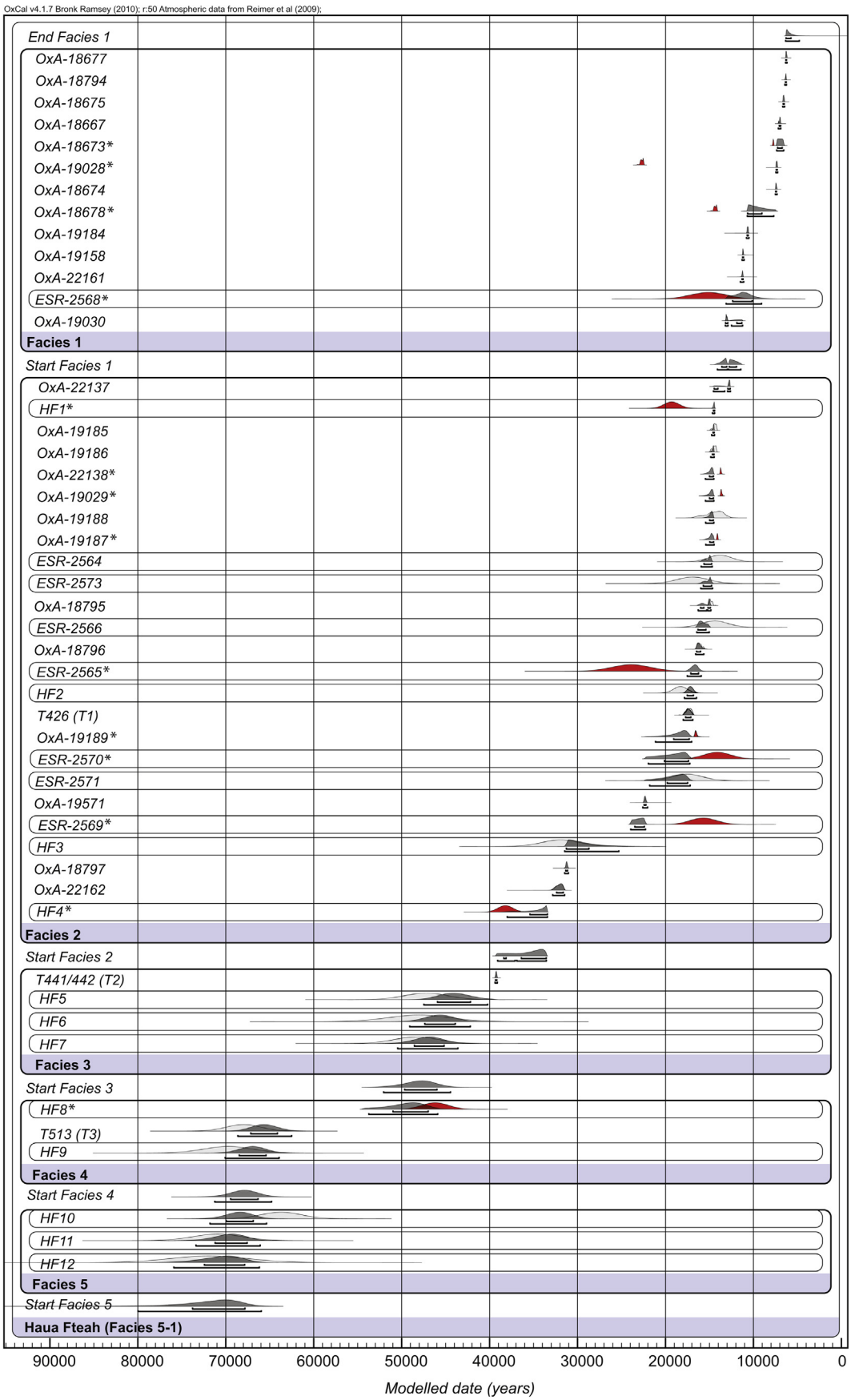

Figure 11. Bayesian model of Haua Fteah age determinations constructed around the five lithostratigraphic facies (Facies 5-1) identified in the sequence (for description see text). Radiocarbon ages from 50 ka BP onwards are calibrated using IntCal09 (Reimer et al., 2009). Older determinations were made with chronometric methods (OSL, ESR), which do not require calibration. The light grey probability distributions represent the calibrated/calculated measurements while in dark grey are the posterior distributions as calculated by the Bayesian model. The determinations classified as outliers are highlighted with an asterisk. Built with OxCal 4.1.7 (Bronk Ramsey, 2009a) (Figure: K. Douka).

significantly smaller than the average errors on the EU and LU estimates, which are in the 1000-years range. Thus, any uncertainties introduced by modelling the uranium uptake history are minor, while at other sites this is often the largest error source for ESR dating of tooth enamel (Grün, 2009a).

The chronostratigraphy of the Middle and Upper Trenches

Using the four dating methods described above, we built a Bayesian statistical framework using the OxCal platform that allows the formal incorporation of external 'prior' information within an explicit probabilistic framework (Bronk Ramsey, 2001, 2009a). The advantage of using such a model is that it may result in the reduction in uncertainty of date estimates for a particular sedimentary facies or cultural phase. It also allows for an assessment of the correspondence between ages obtained using the same and/or different dating methods, and their correspondence to other independent proxies, such as the stratigraphy or archaeological context. The outlier detection analysis as described by Bronk Ramsey (2009b) was used to assess the likelihood of each result being consistent within the constraints of the modelled sequence, thus allowing for the identification of possible erroneous determinations or problematic stratigraphic contexts. An outcome of the model is the creation of a Probability Distribution Function (PDF) between each facies/phase boundary that represents the end and start dates of the corresponding facies/phases.

To maximize the information that we can gain from the chronometric determinations obtained for the Haua Fteah, two sets of priors were used to construct two different Bayesian models. The first model used, as prior information, the five major lithostratigraphic facies defined by the CPP for the site (Fig. 11). The second model built the framework around the cultural phases identified by McBurney, on the basis of the CPP's identification of McBurney's layers in the cleaned faces of his trenches (Fig. 12). In the Discussion section we review the reliability of this cultural phasing as it is being assessed by the new excavations, particularly of Trench M.

The original standardised likelihoods are shown in Figs. 11 and 12 in light shaded grey, while the modelled or posterior probability densities are shown in a darker shade of grey/black. For ^{14}C determinations, the calibrated age ranges are presented, expressed as calendar years before AD 1950 (i.e., cal BP; for the actual ranges see Table 1). The OSL ages are expressed as calendar years before today (i.e., not AD 1950) and do not have fully independent uncertainties associated with their age estimates; many of the errors are shared among all of the OSL ages and are referred to as systematic errors, which may include, for example, calibration errors for the various pieces of equipment that were used (Galbraith and Roberts, 2012). The error estimate unique to each OSL age is called the random error and is predominantly derived from the propagation of measurement uncertainties, which come from counting errors on each parameter measured (dose rate and equivalent dose), fitting uncertainties in D_e estimation, and variation between D_e values from different grains (see earlier discussion). The OSL ages reported in Table 3 include both the random and systematic uncertainties. When ages with common systematic errors and random errors are combined, only the latter should be included, so prior to construction of the Bayesian models, we excluded all systematic errors so that the 95.4% probability distribution for the OSL ages only includes the total random uncertainty associated with each age, following Rhodes et al. (2003).

In the following sections, BP and cal BP are exclusively used for ^{14}C ages (raw and calibrated, respectively), whereas years or thousands of years (ka) are used for all other dating methods. When durations or start and end ages determined using the Bayesian model are reported, and such ages are made up from ages derived using multiple methods, only years or ka are used. Ranges and ages discussed below are reported at the 68.2% confidence interval, and durations of phases at the 95.4% confidence level.

A Bayesian model within a sedimentological framework

The first Bayesian modelled sequence (Fig. 11) was constructed around the five major lithostratigraphic facies defined for the upper 7.5 m of the deposit shown in Fig. 6. Forty-eight new determinations were included: 25 ^{14}C dates on charcoal, 12 OSL determinations, eight ESR measurements, and the correlated ages for the three identified tephras. The ^{14}C (Table 1) and ESR (Table 3) dating results from Trench M excavation were not included, as the major goal of the exercise reported here was to assess the chronological framework of the freshly-exposed sections of the McBurney excavation. We omitted the five 'young' ^{14}C determinations (OxA-18836, OxA-22163, OxA-22165, OxA-22166 and OxA-22232); the historic ^{14}C age at the top of the sequence (OxA-18710); four ^{14}C measurements on marine shell ornaments from the McBurney collection whose precise locations compared to the CPP contexts cannot be defined yet (OxA-21085, OxA-21086, OxA-21087 and OxA-21088); and six ^{14}C determinations for the oldest samples collected, thought to be underestimates of the true age as previously discussed (UBA-16129, UBA-16131–16134 and OxA-22164).

Initially, the determinations were divided in two broad sequences (Facies 5-3 and Facies 2-1) with different resolutions, and several sub-sequences and phases therein. In this first modelling attempt, 13 (~27%) of the 48 ages included in the model were identified as outliers (highlighted with an asterisk in Fig. 11); these were deemed 100–60% outliers and therefore did not contribute much to the constructed chronology. Nevertheless, the rest of the modelled results allowed us to estimate the start and end boundaries, as well as the most probable duration, for the five lithostratigraphic facies. These estimates should be treated with caution as they may change with the addition of further data.

The model indicates that the exposed and dated layers of Facies 5 were deposited between ca.75 and 65 ka, although the start date of Facies 5 is certainly earlier (see below, and Discussion). Facies 4 spans the interval between 68 and 47 ka, but a visual inspection of Fig. 11 reveals that the ages may be consistent with a temporal gap of relatively long duration. An alternative explanation may be that the sediments at the top of Facies 4, dated by OSL sample HF8, are associated with the start of Facies 3. This is in agreement with the sedimentological interpretation, which suggests that the top of Facies 4 is represented by a heavily-weathered layer, suggestive of prolonged surface exposure. HF8, thus, likely dated re-activation of sediment in this layer and initial sediment deposition at the start of Facies 3 rather than the latest deposition of Facies 4. The duration of Facies 3 is modelled during the period from 48 to 34 ka. The likely duration of Facies 2 is modelled between 35 ka and 12 ka. Facies 1b started ca. 13.6–11.9 ka and lasted until the mid-Holocene. Facies 1a continues to the present, and indeed is still accumulating.

In terms of Marine Isotope Stages, the modelled age spans indicate that Facies 5 (as exposed) falls almost completely within the early part of MIS 4 (dated globally to ca. 74–60 ka). Facies 4, beginning at 68 ka, developed from the middle of MIS 4 into MIS 3 (the latter dated globally to ca. 60–24 ka). Facies 2 spanned the latter part of MIS 3 and all of MIS 2 (dated globally to ca. 24–11 ka), and Facies 1 developed during the Holocene. The dating of the upper part of the sequence fits broadly well with the environmental interpretations drawn from stratigraphy: the cooling evidenced by the éboulis-dominated Facies 2 (Fig. 13) is consistent with cooling at the end of MIS3 and into MIS2, and an

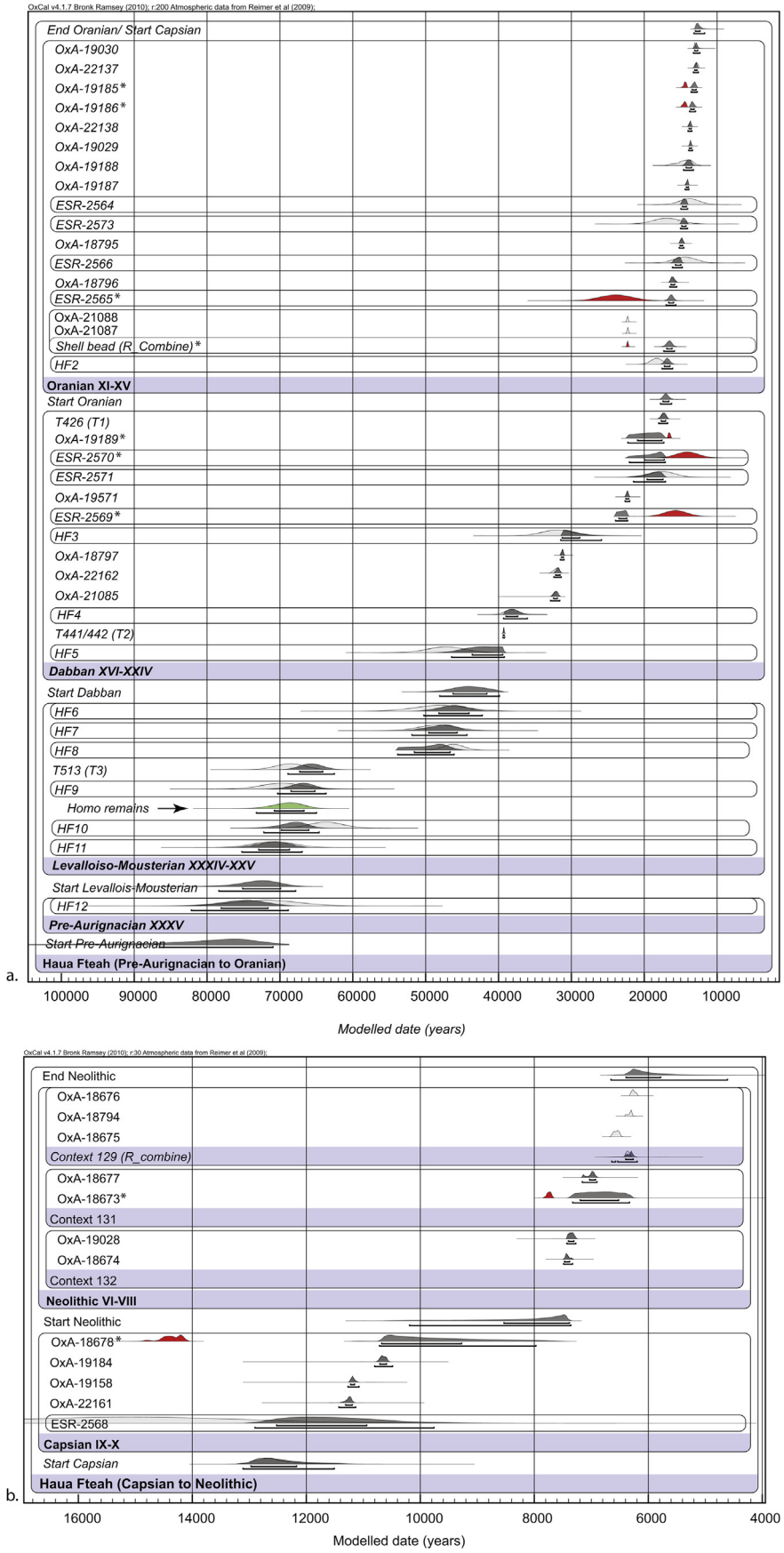

Figure 12. Bayesian model of Haua Fteah constructed around the broad archaeological divisions (Pre-Aurignacian, Levalloiso-Mousterian, Dabban, Oranian, Capsian, Neolithic) and including radiometric determinations (^{14}C, OSL, ESR) and tephra (T) age estimates: (a) Pre-Aurignacian to Oranian; (b) Capsian and Neolithic. Determinations flagged as outliers are highlighted with an asterisk. The probability distribution function (PDF) for the *Homo* remains is plotted in (a) and indicated by an arrow. The radiocarbon measurements were calibrated using IntCal09 (Reimer et al., 2009) and the model was built with OxCal 4.1.7 (Bronk Ramsey, 2009a) (Figure: K. Douka). (For interpretation of the references to colour in this figure legend, the reader is referred to the web version of this article.)

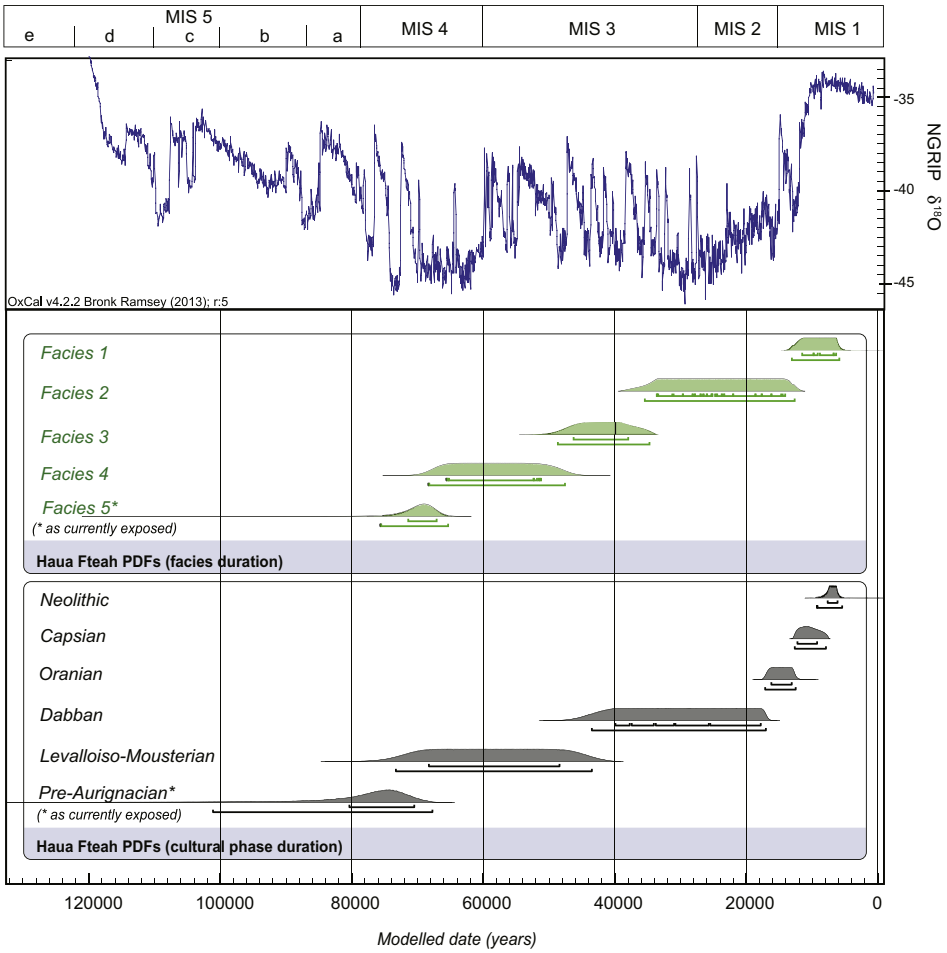

Figure 13. Probability distribution functions (PDFs) for the duration of each facies and for each archaeological phase as modelled in Figs. 11 and 12a and b. The PDFs, the numerical age estimates of which are shown in Table 4, are plotted here below the NGRIP oxygen isotope record. The latter is used as a proxy for temperature variation over the Last Glacial Cycle (North Greenland Ice Core Project members, 2004). The Marine Isotope Stages are also indicated on the top of the plot. Plot generated with OxCal 4.1.7 (Bronk Ramsey, 2009a) (Figure: K. Douka).

overall reduction of physical weathering with the start of Facies 1 is consistent with warming into the Holocene. Towards the bottom of the sequence, however, where the model relies on a relatively restricted number of dates compared with the upper part of the sequence that is supported by multiple dates and methods, there appears to be a slight disjuncture between the modelled dates, their relation to global changes and the environmental interpretations constructed for the facies. According to the model, the relatively homogeneous, silty, Facies 5 identified at the base of the Middle Trench was deposited during the very latter part of MIS 5 and mainly in early MIS 4, but very similar sediments appear to continue into the Deep Sounding for a further depth of ~6.5 m, suggesting that Facies 5 contains at least the latter part of MIS 5 as well as MIS 4. If correct, this would imply that the major global climatic shift that is the end of MIS 5 and the onset of MIS 4 had no impact on the sedimentation processes of the Haua Fteah and that severe cooling only accompanied the end of MIS 4, and is evidenced in the increased physical weathering in Facies 4, which dates to this period. It is possible that this disjuncture highlights a local lag in response in the cave sediments to global environmental change, but it is equally possible that the dating model requires further clarification at this depth before the response of the cave to environmental change can be fully understood.

A Bayesian model within a cultural framework

In a second modelling exercise, we built a framework around the cultural phases proposed by McBurney (1967), and used the correlated CCP contexts and McBurney layers to assign each age to a phase (Fig. 12a,b). In this model, 50 age determinations were used. The same samples that were excluded in the previous model were excluded again, and in addition OSL HF1 was also left out as being too old. Three ^{14}C dates on marine shell ornaments from McBurney's excavations (OxA-21085, OxA-21087, OxA-21088) were included this time within the respective archaeological layers. OxA-21086 was not modelled because its precise location in the stratigraphy cannot be established. The model is shown in Fig. 12 with the ten outliers (~20% of the 50 ages) marked in black. As previously, we have calculated the duration of each cultural phase, which is essentially a probability distribution function between the start and end phase boundaries (Fig. 13).

The top of McBurney's earliest archaeological phase, the Pre-Aurignacian, has a single OSL age of 71.9 ± 7.6 ka for sample HF12 that was collected from the bottom of the Middle Trench, equivalent to his Layer XXXV (Table 4; Fig. 6). A new series of OSL samples was collected from the cleaned faces of the Deep Sounding after emptying its backfill in 2012, but the results from these are not yet available, so the start date and duration of the Pre-Aurignacian

Table 4
The chronology of prehistoric occupation in the Haua Fteah, according to the original study (McBurney, 1967) and the results of the Bayesian statistical modelling of the new determinations (^{14}C, tephra, OSL, ESR). In the latter case, proposed modelled ages quoted here were generated from the probability distribution functions for each cultural phase and correspond to their most likely duration at 68.2% and 95.4% level of confidence.

Phase	Layers	Estimated age (McBurney, 1967) (ka)	Proposed age (this study) (ka)	
			68.2%	95.4%
Pre-Aurignacian	XXXV and below	80–65	80.3–70.5[a]	101.6–67.7
Levalloiso-Mousterian	XXXIV–XXV	65–40	68.1–48.7	73.3–43.5
Dabban	XXV–XVI	40–15	40.0–18.1	43.5–17.1
Oranian	XV–XI	15–10	16.1–13.1	17.2–12.5
Capsian	X, IX	10–7	12.3–9.3	12.7–7.9
Neolithic	VIII–IV	7–4.7	7.7–6.2	9.3–5.4

[a] The beginning of the Pre-Aurignacian is likely to extend much earlier than this; see text for discussion.

archaeological phase currently remain unknown (see Discussion, below).

The Levalloiso-Mousterian phase (McBurney's Layers XXXIV to XXV) is dated by six OSL samples and the tephra concentration HF_T513/T3 in Context 513, which we correlated with Layer XXX. In the Lago Grande di Monticchio record, this tephra was dated at 68.6 ± 2.1 ka (Wulf et al., 2007). While OSL sample HF8 from the same context is not identified as a certain outlier due to the specifics of the model, it is much younger; the reasons for this were discussed earlier (see 'OSL dating'). All of the other determinations demonstrate good agreement in relation to their relative stratigraphic positions. The modelling suggests a start date for the Levalloiso-Mousterian phase at some point between 75 and 70 ka (Fig. 12a) and that it lasted for about 30 ka, from 73 to 43 ka (Table 4). Based on a visual inspection of the age distributions within this phase (Fig. 12a), it may be possible to suggest that it occurred at two statistically-distinct time periods, from ~73 to 64 ka and from ~52 to 44 ka. The most likely age of the two modern human mandibles found in the Levalloiso-Mousterian Layer XXXIII is placed between 73 and 65 ka BP at the 95.4% confidence level (Fig. 12a: in green).

In our model, the start and the end of the Dabban are bracketed by the ^{39}Ar/^{40}Ar age of 39.30 ± 0.11 ka (68.2%) for the Campanian Ignimbrite and the ^{14}C age for the Biancavilla Ignimbrite of 17,670–17,070 cal BP. McBurney (1967) sub-divided the Dabban into an early and a late phase, obtaining five dates for its total duration, three for the former and two for the latter (SOM Table S1). When calibrated, these dates indicated that the Early Dabban fell between 39 and 32 ka BP and the Late Dabban between 22 and 19 ka BP. Our modelled results broadly agree with McBurney's findings: the duration of the Dabban is calculated to be between 40 and 18 ka (65.4%, ~22 ka) or from 43 to 17 ka (95.4%, ~26 ka), not too dissimilar to the ca. 20 ka duration calculated by McBurney (1967) (but see Discussion concerning the Levalloiso-Mousterian/Dabban transition).

The start date for the Oranian (McBurney's Layers XV–XI) is calculated between 17.0 and 16.0 ka (68.2%), the end at some point shortly after 13 ka and, therefore, its duration between 17.0 and 12.5 ka. This age range is older than McBurney's estimate of 15–10 ka by about two to three millennia (Table 4).

McBurney (1967) judged the Capsian (in Layers X and IX) to be an entirely Holocene or Mesolithic phenomenon, dating it to ca. 10–7 ka (SOM Table S1). The new model places its beginnings at 12.9–12.3 ka in the terminal Pleistocene and its duration between 12.6 and 7.9 ka.

The start boundary of the Neolithic is rather long (8.5–7.4 ka cal BP), but the earliest direct determinations place Contexts 132–131, which are the equivalent to McBurney's Layer VIII ('Pottery Neolithic'), at about 7.4–6.9 ka cal BP. This agrees rather well with the two determinations that McBurney obtained for this layer (SOM Table S1: NPL-42 and W-98), which, despite the much larger associated errors, when calibrated fall between 8.0 and 7.1 ka cal BP. His latest Neolithic dates, from Layer VI, which span between 6.7 and 5.4 ka BP, compare with our own estimate of ca. 6.4–6.2 ka BP for Context 129 (on the basis of a single sample) or about 6.4–5.8 ka BP for the latest phase of Neolithic activity overlain by the construction of the Graeco-Roman structure.

Discussion

The age of the initial use of the site can only be estimated tentatively so far because our earliest date is the OSL determination from the base of the Middle Trench. This corresponds to the top of the Pre-Aurignacian sequence defined by McBurney (1967), who found Pre-Aurignacian material in the underlying 5.5 m of the Deep Sounding, including near its base. Moreover, the CPP excavations in 2012 found a further ~1 m of undisturbed sediment at the base of the Deep Sounding with further, albeit scarce, evidence for human occupation below where McBurney ceased excavation. This included a small number of struck and retouched flakes and bladelets, micro-debitage, marine shell including burnt fragments of *Osilinus turbinatus*, and burnt fragments of land snails such as *H. melanostoma*, both significant food sources in the Oranian and Capsian phases of occupation (Barker et al., 2012). The rather uniform sedimentary characteristics of the Deep Sounding profiles, including the newly excavated basal sediments, suggest that the Deep Sounding sediments probably accumulated within MIS 5 (Barker et al., 2012; Fig. 13).

The two modern human mandibles (Hublin, 2000) were found in Layer XXXIII near the base of the Levalloiso-Mousterian occupation, and there is good reason to suppose that modern humans were responsible for the Pre-Aurignacian material in the cave as well. The latter was primarily found in the base of the Deep Sounding, which in total removed ~8.75 m^3 of sediment, whereas the Levalloiso-Mousterian material was collected from ~30.00 m^3 of sediment in the lower part of the Middle Trench. Ongoing analysis of the Pre-Aurignacian and Levalloiso-Mousterian lithic assemblages in the McBurney Archive suggests that they are more likely to be sampling variants rather than distinct industries (Reynolds, 2012): all of the elements of the Pre-Aurignacian occur with variable degrees of expression in the Levalloiso-Mousterian. Marine molluscs are a frequent part of the fauna associated with the Pre-Aurignacian lithics and both these and fish and crab remains were recovered from the excavation at the base of the Deep Sounding (Barker et al., 2012), so it is possible that the Pre-Aurignacian is a littoral or coastal variant of a more general Middle Palaeolithic (or Middle Stone Age [MSA], to use the African terminology) adaptation in the Gebel Akhdar. A probable worked bone point was recovered from a Pre-Aurignacian level in the Deep Sounding in 2012 (Barker et al., 2012), adding to the worked bones in MSA contexts at Dar es-Soltan 1 (Ruhlmann, 1951) and El Mnasra (Hajraoui, 1994) as evidence of the use of this technology on the North African littoral at a time not dissimilar to its appearance along the coast in southern Africa where, like coastal exploitation strategies, it is associated with early modern humans (Henshilwood and Sealy, 1997; Henshilwood et al., 2001).

In recent years, the Aterian, an MSA industry that contains tanged pieces, blades, bladelets, and bifacial foliates with reduction that frequently involves small Levallois radial cores, sometimes associated with shell beads and pigments (Scerri, 2012), has

been regarded as a significant marker of the appearance of modern humans in North Africa (Garcea, 2004, 2009, 2010c; Bouzouggar et al., 2007; Dibble et al., 2013), having been found in association with modern human fossils at Mugharet el Aliya (Wrinn and Rink, 2003), Dar es-Soltan I (Barton et al., 2009), Contrebandiers (Nespoulet et al., 2008; Dibble et al., 2012) and Zouhrah (Trinkhaus, 2005; Fig. 1). Dates for the Aterian range from ca. 60–90 ka in the Sahara (Cremaschi et al., 1998) and ca. 85–43 ka in the Gebel Gharbi mountains of Tripolitania, western Libya (Garcea, 2010c) to greater than 100 ka in the Maghreb (Barton et al., 2007, 2009; Richter et al., 2010; Schwenninger et al., 2010; Jacobs et al., 2011, 2012; Clark-Balzan et al., 2012). McBurney said at different times that the Aterian was both present and not present at the Haua Fteah, in part reflecting the continuing difficulties arising from the use of the term to describe the occurrence of either a few 'classic types' such as tanged pieces or a much larger repertoire of forms. The re-analysis of the MSA material in the archive indicates that there is a consistent but low frequency presence of elements that could be considered Aterian but nothing to define an assemblage as Aterian (Reynolds, 2012; Scerri, 2012). Isolated tanged pieces have been found by the CPP project in the environs of the cave and an industry with pedunculates was excavated in the Hagfet et-Tera cave at the western edge of the Gebel Akhdar, ~175 km from the Haua Fteah (McBurney and Hey, 1955; McBurney, 1960).

It has been suggested that the first systematic occupation of North Africa by modern humans was probably as a result of a northward movement across the Sahara in MIS 5, when wetter climates created a string of major lakes across what is now desert (Armitage et al., 2007; Osborne et al., 2008; Garcea, 2010c; Drake et al., 2011). Given the topographic isolation of the Gebel Akhdar, separated from the Maghreb by the hyper-arid Gulf of Sirte desert, there is at least as strong a case for Egypt and/or the Levant (where early modern humans at Qafzeh and Skhul possibly date to ca. 130–70 ka, Shea, 2010) as the source for the Haua Fteah's modern humans. Their estimated age of 73–65 ka would place them within MIS 4, a period when the Qafzeh/Skhul hominins might have retreated to coastal refugia such as coastal North Africa (the Gebel Akhdar) and Arabia in response to overpopulation or climate change (Beyin, 2011).

Layer XXV, McBurney's transitional layer between the Levalloiso-Mousterian and the blade-based Dabban assemblages, is now dated to between 46 and 41 ka (Fig. 13: Dabban start boundary), well before the CI eruption, the products of which have been found in the cave. A start date for the Dabban at this time would be similar to the current dates for the first appearance of Upper Palaeolithic technologies in the Levant (Rebollo et al., 2011), Southern Europe (Benazzi et al., 2011) and Central and Northern Europe (Higham et al., 2011), with an important bearing on theories about the timing and direction of the spread of modern humans equipped with these technologies, including whether they spread from North Africa into the Levant or vice versa (Olivieri et al., 2006; Iovita, 2009).

However, it should be emphasised that the character and timing of the transition between the two industries are unclear. Layer XXV was dug in two spits (spits 32 and 33: Fig. 3, right image). McBurney (1967: 125) noted the presence of both Levalloiso-Mousterian and Dabban material in both spits, the greater frequency of the latter in the upper spit, but also the occurrence of occasional "more or less Levalloisoid" flakes in the overlying Level XXIV, which he regarded as likely to be intrusions from Layer XXV. The Trench M excavations have just reached this part of the stratigraphy and clarifying whether the transition from Levalloiso-Mousterian to Dabban technologies was gradual or sudden is an important focus of the new work.

It is apparent from the depth distribution of lithics recorded by McBurney, and also noted in Trench M, that despite its long duration the Dabban, like the Levalloiso-Mousterian, in fact consisted of subphases of activity separated by short, but distinct, temporal gaps. Its restriction to the Gebel Akhdar suggests that the latter, surrounded today by desert to the east, south, and west, is likely to have been a refuge for human populations during the oscillating climatic regime of MIS 3 and the prolonged period of cooling and associated aridity and landscape degradation that characterized MIS 2.

McBurney (1967) dated the first use of microlithic Oranian technologies at the site to ca. 14 ka, but the new model suggests that they started ca. 17–16 ka, coinciding with the beginnings of deglaciation after the peak of LGM conditions (North Greenland Ice Core Project members, 2004). Oranian technologies continued to be used at the cave until ca. 13–12 ka. Iberomaurusian microlithic technologies like the Oranian are evidenced in the Maghreb by ca. 26 ka (Barton et al., 2007; Bouzouggar et al., 2008) and in the Gebel Gharbi by ca. 20 ka (Garcea, 2010b). The time lapse in the appearance of microlithic technologies is at variance with theories of the Maghrebian Iberomaurusian having its origins in a westward migration of people from the Gebel Akhdar (e.g., Close and Wendorf, 1990; Pereira et al., 2010).

The Capsian phase at the Haua Fteah was dated by McBurney (1967) to between 10 and 7 ka. Our new chronological framework places its duration from 12.6 to 7.9 ka, so through the Younger Dryas cold stage into the Holocene. McBurney attributed the development of the Capsian across North Africa to population movements, but like the Oranian, from which it clearly developed, it seems more likely that it was primarily a behavioural response to climate change. In the Haua Fteah, there is evidence for subsistence diversification during the Younger Dryas: the hunting of Barbary sheep, gazelle (*Gazella* sp.) and hartebeest (*Alcelaphus* sp.); fishing; the collecting of crustaceans, marine molluscs and land snails; and the gathering of a range of plant foods including pine cones (which were stored), large-seeded legumes, fruits and berries (Barker et al., 2010). A possible interpretation of root etching on the butchery waste recovered from Trench M (indicating the growth of vegetation on discarded bones), and of the lack of trampling damage, is that the Early Capsian occupation of the cave was markedly seasonal. Changes in the size and abundance of *Osilinus* and *Patella* sp. shells indicate severe resource pressure or 'overgathering' from food scarcity at this time (Hunt et al., 2011).

The period after the 8.2 ka event (Weninger et al., 2006) does not seem to have been significantly drier at the Haua Fteah than the period before it, the land snail assemblages do not point to significant aridification (Hunt et al., 2011), and there does not seem to be a strong link between the 8.2 ka event and subsistence change as has been argued for in the eastern Mediterranean (Weninger et al., 2006) and the Maghreb (Jackes and Lubell, 2008). The first appearance of Neolithic pottery at the cave is now dated to ca. 7.4–6.9 ka, not dissimilar to McBurney's dates for this layer (VIII) of 8.0–7.1 ka (McBurney, 1967). Rather than a package of new resources, technologies, and associated behaviours appearing at the site at this time, there is evidence for piecemeal change, as appears to be the case elsewhere in North Africa (Linstädter, 2008; Dunne et al., 2012; Barker, 2013). The landscape around the site at this time was relatively open scrubland (Hunt et al., 2011). People continued to hunt species such as Barbary sheep and collect land snails (*Trochoidea* spp., *Eobania* spp., *H. melanostoma*) and marine molluscs (*Patella caerulea*, *O. turbinatus*), making fine drills ('mèche de foret') likely used as picks for removing the latter from their shells (Barker et al., 2012). There are less marked signs of resource stress in the land snails and marine molluscs (Hunt et al., 2011). This system of foraging, more or less a continuation of Capsian practices in the Early Holocene, was augmented at some stage in the Neolithic by sheep

and goat herding (Klein and Scott, 1986), but there is no certain evidence for cereal cultivation in terms of directly-dated seeds. Later Neolithic occupation of the cave was more intensive and probably involved the stabling of animals as well as middening (Hunt et al., 2010). Whether the end of Neolithic occupation at the site ca. 6.2–5.8 ka was related to the aridification that was widespread in the eastern Sahara at this time (Kuper and Kropelin, 2006; Cremaschi et al., 2010) is unclear. The really significant transformation in land use was in the Graeco-Roman period, when the cave was used for stabling livestock, as today, and there is evidence in its sediments and palynology for significant impacts on the landscape beyond the cave from ploughing and cultivation (Hunt et al., 2010).

Conclusions

Ever since the 1950s excavations by Charles McBurney, the Haua Fteah has held iconic status in North African prehistory because of its deep sequence of occupation. Yet several aspects of the character of its geological and archaeological sequences have remained unclear, and their chronology has been based on very early chronometric determinations, which required urgent revisiting. New work has been able to identify the McBurney layers in the well-preserved faces of his trenches and compare these with the stratigraphic units observed in the newly-recorded sections, and date the layers that McBurney linked to the major cultural phases of human occupation that he defined.

The project has still to fully characterize and date the sediments of the Deep Sounding, ~7.5–14.0 m below the present ground surface (Fig. 3), but the results of analysing the first main set of dating materials collected from the cleaned faces of the Middle and Upper Trenches (charcoal and land snails for ^{14}C dating; tephras; sediments for OSL dating; and animal teeth for ESR dating) and marine molluscs (shell beads) from the 1950s archives, using a Bayesian statistical approach, have demonstrated that five major sedimentary facies can be recognised and that the upper four of these developed during MIS stages 4–1, though (apart from the Holocene Facies 1) not in strict synchroneity.

New excavations down the side of the McBurney trenches are not yet complete, but the preliminary findings of the project are that: (1) the major cultural units that he recognised (Pre-Aurignacian, Levalloiso-Mousterian, Dabban, Oranian, Capsian, Neolithic, Graeco-Roman, Modern) are appropriate except that the first two are likely to be sampling variants rather than distinct industries, (2) the two modern human mandibles have been dated to ca. 73–65 ka at the 95.4% confidence level, so within MIS 4, (3) the first appearance of the Upper Palaeolithic Dabban industry dates to ca. 43–40 ka BP, below Campanian Ignimbrite tephra dated to ca. 39 ka BP, but the character of the transition from the Levalloiso-Mousterian is not yet clarified, (4) the first microlithic (Oranian) technologies date to soon after the peak of LGM conditions, (5) the increasingly microlithic Capsian developed in the Younger Dryas, (6) Neolithic pottery first appeared ca. 7.4–6.9 ka and sheep and goat herding somewhat later (not yet accurately dated), both being integrated within Capsian foraging systems, whereas the first evidence for plant cultivation is not until the Graeco-Roman period. The revised chronostratigraphy of the Haua Fteah, now dated with a precision unavailable to the original excavator, confirms the site as a reference sequence for North African prehistory, and for potential interactions between Africa, the Levant and Europe, from the first appearances of *Homo sapiens* to the spread of farming.

Acknowledgements

GB would like to acknowledge in particular the permission of the Department of Antiquities of Libya to undertake the project, and its logistical support; and the financial support of the European Research Council (Advanced Investigator Grant 230421: TRANS-NAP project: Cultural Transformations and Environmental Transitions in North African Prehistory), the Society for Libyan Studies, the Leakey Foundation, and the Natural Environment Research Council (NERC Radiocarbon Facility). KD was funded by the Leverhulme Trust project AHOB3. CL, VC, PA and ET were funded by the UK Natural Environment Research Council consortium RESET (NE/E015670/1 and NE/E015905/1) and would like to thank Victoria Smith for the tephra EPMA. ZJ and RGR were supported by Australian Research Council grants DP1092843 to ZJ and DP0666084 to RR, RG, and ZJ. RI was supported by a UK Arts and Humanities Research Council doctoral award and Magdalene College, Cambridge. Tom Higham should be thanked for assistance with the radiocarbon dating programme at Oxford. Contributor roles: KD: Bayesian modelling; ZJ, RGR: OSL dating; CL, ET, PA, VC, SW: tephrochronology; RG, LK, MA: ESR dating; LF: geoarchaeology; RI: geomorphology, micromorphology; CH: geomorphology, molluscan analysis; TR: excavation director, lithic analyses; EH: molluscan analysis; GB: project director.

Appendix A. Supplementary material

Supplementary data related to this article can be found online at http://dx.doi.org/10.1016/j.jhevol.2013.10.001.

References

Albert, P., Tomlinson, E., Smith, V.C., Di Roberto, A., Todman, A., Rosi, M., Marani, M., Müller, W., Menzies, M., 2012. Marine–continental tephra correlations: volcanic glass geochemistry from the Marsili Basin and the Aeolian Islands, Southern Tyrrhenian Sea. J. Volcanol. Geotherm. Res. 229–230, 74–94.

Albert, P.G., Tomlinson, E.L., Lane, C.S., Wulf, S., Smith, V.C., Coltelli, M., Keller, J., Lo Castro, D., Manning, C.J., Müller, W., Menzies, M.A., 2013. Late glacial explosive activity on Mount Etna: implications for proximal–distal tephra correlations and the synchronisation of Mediterranean archives. J. Volcanol. Geotherm. Res. 265, 9–26.

Armitage, S.J., Drake, N.A., Stokes, S., El-Hawat, A., Salem, M.J., White, K., Turner, P., McLaren, S.J., 2007. Multiple phases of North African humidity recorded in lacustrine sediments from the Fazzan Basin, Libyan Sahara. Quatern. Geochronol. 2, 181–186.

Arnold, L.J., Roberts, R.G., 2009. Stochastic modelling of multi-grain equivalent dose (De) distributions: implications for OSL dating of sediment mixtures. Quatern. Geochronol. 4, 204–230.

Arnold, L.J., Roberts, R.G., Galbraith, R.F., DeLong, S.B., 2009. A revised burial dose estimation procedure for optical dating of young and modern-age sediments. Quatern. Geochronol. 4, 306–325.

Barker, G., 2006. The Agricultural Revolution in Prehistory: Why Did Foragers Become Farmers? Oxford University Press, Oxford.

Barker, G., 2013. The Neolithisation of northeastern Africa: reflections on knowns, unknowns, and unknown unknowns. In: Shirai, N. (Ed.), Neolithisation of Northeast Africa, Studies in Early Near Eastern Production, Subsistence, and Environment, 16. Ex Oriente, Berlin, pp. 249–256.

Barker, G., Hunt, C., Reynolds, T., 2007. The Haua Fteah, Cyrenaica (northeast Libya): renewed investigations of the cave and its landscape, 2007. Libyan Stud. 38, 93–114.

Barker, G., Basell, L., Brooks, I., Burn, L., Cartwright, C., Cole, F., Davison, J., Farr, L., Hamilton, R., Hunt, C., Inglis, R., Jacobs, Z., Leitch, V., Morales, J., Morley, I., Morley, M., Pawley, S., Pryor, A., Rabett, R., Reynolds, T., Roberts, R., Simpson, D., Stimpson, C., Touati, M., der Veen, M., 2008. The Cyrenaican Prehistory Project 2008: the second season of investigations of the Haua Fteah cave and its landscape, and further results from the initial 2007 fieldwork. Libyan Stud. 39, 175–222.

Barker, G., Antoniadou, A., Barton, H., Brooks, I., Candy, I., Drake, N., Farr, L., Hunt, C., Ibrahim, A.A., Inglis, R., Jones, S., Morales, J., Morley, I., Mutri, G., Rabett, R., Reynolds, T., Simpson, D., Twati, M., White, K., 2009. The Cyrenaican Prehistory Project 2009: the third season of investigations of the Haua Fteah cave and its landscape, and further results from the 2007–2008 fieldwork. Libyan Stud. 40, 1–41.

Barker, G., Antoniadou, A., Armitage, S., Brooks, I., Candy, I., Connell, K., Douka, K., Drake, N., Farr, L., Hill, E., Hunt, C., Inglis, R., Jones, S., Lane, C., Lucarini, G., Meneely, J., Morales, J., Mutri, G., Prendergast, A., Rabett, R., Reade, H., Reynolds, T., Russell, N., Simpson, D., Smith, B., Stimpson, C., Twati, M., White, K., 2010. The Cyrenaican Prehistory Project 2010: the fourth season of investigations of the Haua Fteah cave and its landscape, and further results from the 2007–2000 fieldwork. Libyan Stud. 41, 63–88.

Barker, G., Bennett, P., Farr, L., Hill, E., Hunt, C., Lucarini, G., Morales, J., Mutri, G., Prendergast, A., Pryor, A., Rabett, R., Reynolds, T., Twati, M., 2012. The Cyrenaican Prehistory Project 2012: the fifth season of investigations of the Haua Fteah cave. Libyan Stud. 43, 115–136.
Barton, R.N.E., Bouzouggar, A., Collcutt, S., Gale, R., Higham, T.F.G., Humphrey, L.T., Parfitt, S.A., Rhodes, E.J., Stringer, C., Malek, F., 2005. The late Upper Palaeolithic occupation of the Moroccan northwest Maghreb during the Last Glacial Maximum. Afr. Archaeol. Rev. 22, 77–100.
Barton, R.N.E., Bouzouggar, A., Bronk-Ramsey, C., Collcutt, S., Higham, T.F.G., Humphrey, L.T., Parfitt, S.A., Rhodes, E.J., Schwenninger, J.-L., Stringer, C., Turner, E., Ward, S., 2007. Abrupt climatic change and chronology of the Upper Palaeolithic in northern and eastern Morocco. In: Mellars, P., Boyle, K., Bar-Yosef, O., Stringer, C. (Eds.), Rethinking the Human Revolution. McDonald Institute for Archaeological Research, Cambridge, pp. 177–186.
Barton, R.N.E., Bouzouggar, A., Collcutt, S., Schwenninger, J.-L., Clark-Balzan, L., 2009. OSL dating of the Aterian levels at Grotte de Dar es-Soltan I (Rabat, Morocco) and possible implications for the origins of modern *Homo sapiens*. Quatern. Sci. Rev. 28, 1914–1931.
Benazzi, S., Douka, K., Fornai, C., Bauer, C.C., Kullmer, O., Svoboda, J., Pap, L., Mallegni, F., Bayle, P., Coquerelle, M., Condemni, S., Ronchitelli, A., Harvati, K., Weber, G.W., 2011. Early dispersal of modern humans in Europe and implications for Neanderthal behavior. Nature 479, 525–528.
Beyin, A., 2011. Upper Pleistocene human dispersals out of Africa: a review of the current state of the debate. Int. J. Evol. Biol., 1–17, 615094.
Bird, M., Ayliffe, L.K., Fifield, K., Cresswell, R., Turney, C., 1999. Radiocarbon dating of 'old' charcoal using a wet oxidation-stepped combustion procedure. Radiocarbon 41 (2), 127–140.
Blockley, S.P.E., Pyne-O'Donnell, S.D.F., Lowe, J.J., Matthews, I.P., Stone, A., Pollard, A.M., Turney, C.S.M., Molyneux, E.G., 2005. A new and less destructive laboratory procedure for the physical separation of distal glass tephra shards from sediments. Quatern. Sci. Rev. 24, 1952–1960.
Bouzouggar, A., Barton, R.N.E., Vanhaeren, M., D'Errico, F., Collcutt, S., Higham, T., Hodge, E., Parfitt, S., Rhodes, E., Schwenninger, J.-L., Stringer, C., Turner, E., Ward, S., Moutmir, A., Stambouli, A., 2007. 82,000-year-old shell beads from North Africa and implications for the origins of modern human behaviour. Proc. Natl. Acad. Sci. 104, 9964–9969.
Bouzouggar, A., Barton, R.N.E., Blockley, S., Bronk-Ramsey, C., Collcutt, S.N., Gale, R., Higham, T.F.G., Humphrey, L.T., Parfitt, S., Turner, E., Ward, S., 2008. Reevaluating the age of the Iberomaurusian in Morocco. Afr. Archaeol. Rev. 25, 3–19.
Bridges, E.M., 1997. World Soils, Third edition. Cambridge University Press, Cambridge.
Brock, F., Higham, T.F.G., Ditchfield, P., Bronk Ramsey, C., 2010. Current pretreatment methods for AMS radiocarbon dating at the Oxford Radiocarbon Accelerator Unit (ORAU). Radiocarbon 52 (1), 103–112.
Bronk Ramsey, C., 2001. Development of the radiocarbon calibration program OxCal. Radiocarbon 43 (2A), 355–363.
Bronk Ramsey, C., 2009a. Bayesian analysis of radiocarbon dates. Radiocarbon 51 (1), 337–360.
Bronk Ramsey, C., 2009b. Dealing with outliers and offsets in radiocarbon dating. Radiocarbon 51 (3), 1023–1045.
Callow, W.J., Baker, M.J., Pritchard, D.H., 1963. National physics laboratory radiocarbon measurements I. Radiocarbon 5, 34–38.
Clark-Balzan, L.A., Candy, I., Schwenninger, J.-L., Bouzzouggar, A., Blockley, S., Nathan, R., Barton, R.N.E., 2012. Coupled U-series and OSL dating of a Late Pleistocene cave sediment sequence, Morocco, North Africa: significance for constructing Palaeolithic chronologies. Quatern. Geochronol. 12, 53–64.
Close, A., Wendorf, F., 1990. North Africa at 18,000 BP. In: Gamble, C., Soffer, O. (Eds.), The World at 18,000 BP, Low Latitudes, Volume II. Unwin Hyman, London, pp. 41–57.
Coltelli, M., Del Carlo, P., Vezzoli, L., 2000. Stratigraphic constraints for explosive activity in the past 100 ka at Etna Volcano, Italy. Int. J. Earth Sci. 89 (3), 675–677.
Costa, A., Folch, A., Macedonio, G., Giaccio, B., Isaia, R., Smith, V.C., 2012. Quantifying volcanic ash dispersal and impact of the Campanian Ignimbrite super-eruption. Geophys. Res. Lett. 39, L10310.
Cremaschi, M., Di Lernia, S., Garcea, E., 1998. Some insights on the Aterian in the Libyan Sahara: chronology, environment, and archaeology. Afr. Archaeol. Rev. 15, 261–286.
Cremaschi, M., Zerboni, A., Spotl, C., Felletti, F., 2010. The calcareous tufa in the Tadrart Acacus Mt. (SW Fezzan, Libya): an early Holocene palaeoclimate archive in the central Sahara. Palaeogeogr. Palaeoclimatol. Palaeoecol. 287, 81–94.
Deniel, C., Aydar, E., Gourgaud, A., 1998. The Hasan Dagi stratovolcano (Central Anatolia, Turkey): evolution from calc-alkaline to alkaline magmatism in a collision zone. J. Volcanol. Geotherm. Res. 87, 275–302.
De Vivo, B., Rolandi, G., Gans, P.B., Calvert, A., Bohrson, W.A., Spera, F.J., Belkin, H.E., 2001. New constraints on the pyroclastic eruptive history of the Campanian volcanic Plain (Italy). Mineral. Petrol. 73, 47–65.
Dibble, H.L., Aldeias, V., Alvarez-Fernández, E., Blackwell, B., Hallett-Desguez, E., Jacobs, Z., Goldberg, P., Morala, A., Meyer, M.C., Olszewski, D.I., Reed, K., Reed, D., Richter, D., Roberts, R.G., Sandgathe, D., Schurmans, U., Skinner, A., El-Hajraoui, M., 2012. New excavations at the site of Contrabandiers Cave, Morocco. Paleoanthropology, 145–201.
Dibble, H.L., Aldeias, V., Jacobs, Z., Olszewski, D.I., Rezek, Z., Lin, S.C., Alvarez-Fernández, E., Barshay-Szmidt, C.C., Hallett-Desguez, E., Reed, D., Reed, K., Richter, D., Steele, T.E., Skinner, A., Blackwell, B., Doronicheva, E., El-Hajraoui, M., 2013. On the industrial attributions of the Aterian and Mousterian of the Maghreb. J. Hum. Evol. 64, 194–210.
Di Vito, M.A., Sulpizio, R., Zanchetta, G., D'Orazio, M., 2008. The late Pleistocene pyroclastic deposits of the Campanian Plain: new insights into the explosive activity of Neapolitan volcanoes. J. Volcanol. Geotherm. Res. 177, 19–48.
Douka, K., Hedges, R.E.M., Higham, T.F.G., 2010a. Improved AMS ^{14}C dating of shell carbonates using high-precision X-Ray Diffraction (XRD) and a novel density separation protocol (CarDS). Radiocarbon 52 (2–3), 735–751.
Douka, K., Higham, T., Sinitsyn, A., 2010b. The influence of pretreatment chemistry on the radiocarbon dating of Campanian Ignimbrite-aged charcoal from Kostenki 14 (Russia). Quatern. Res. 73, 583–587.
Drake, N., Blench, R.M., Armitage, S.J., Bristow, C.S., White, K., 2011. Ancient watercourses and biogeography of the Sahara explain the peopling of the desert. Proc. Natl. Acad. Sci. 108, 458–462.
Dunne, J., Evershed, R.P., Salque, M., Cramp, L., Bruni, S., Ryan, K., Biagetti, S., di Lernia, S., 2012. First dairying in green Saharan Africa in the fifth millennium BC. Nature 486, 390–394.
Galbraith, R.F., 1988. Graphical display of estimates having differing standard errors. Technometrics 30, 271–281.
Galbraith, R.F., 1990. The radial plot: graphical assessment of spread in ages. Nucl. Tracks Radiat. Meas. 17, 207–214.
Galbraith, R.F., Roberts, R.G., 2012. Statistical aspects of equivalent dose and error calculation and display in OSL dating: An overview and some recommendations. Quatern. Geochronol. 11, 1–27.
Galbraith, R.F., Roberts, R.G., Laslett, G.M., Yoshida, H., Olley, J.M., 1999. Optical dating of single and multiple grains of quartz from Jinmium rock shelter, northern Australia: Part I, experimental design and statistical models. Archaeometry 41, 339–364.
Garcea, E.A.A., 2004. Crossing deserts and avoiding seas: Aterian North African–European relations. J. Anthropol. Res. 60, 27–53.
Garcea, E.A.A., 2009. The evolution and revolutions of the Late Middle Stone Age and Lower Later Stone Age in north-west Africa. In: Camps, M., Szmidt, C. (Eds.), Turning Points and New Directions. Oxbow Books, Oxford, pp. 51–66.
Garcea, E.A.A. (Ed.), 2010a. South-Eastern Mediterranean Peoples Between 130,000 and 10,000 Years Ago. Oxbow Books, Oxford.
Garcea, E.A.A., 2010b. The lower and upper Later Stone Age of North Africa. In: Garcea, E.A.A. (Ed.), South-Eastern Mediterranean Peoples Between 130,000 and 10,000 Years Ago. Oxbow Books, Oxford, pp. 54–65.
Garcea, E.A.A., 2010c. The spread of Aterian peoples in North Africa. In: Garcea, E.A.A. (Ed.), South-Eastern Mediterranean Peoples Between 130,000 and 10,000 Years Ago. Oxbow Books, Oxford, pp. 37–53.
Garcea, E.A.A., 2011. Successes and failures of human dispersals from North Africa. Quatern. Int. 270, 119–128.
Goldberg, P., 1992. Micromorphology, soils and archaeological sites. In: Holliday, V.T. (Ed.), Soils in Archaeology: Landscape Evolution and Human Occupation. Smithsonian Institution Press, Washington, pp. 145–167.
Goodfriend, G.A., Stipp, J.J., 1983. Limestone and the problem of radiocarbon dating of land-snail shell carbonate. Geology 11, 575–577.
Grün, R., 2000. An alternative for model for open system U-series/ESR age calculations: (closed system U-series)-ESR, CSUS-ESR. Ancient TL 18, 1–4.
Grün, R., 2009a. The relevance of parametric U-uptake models in ESR age calculations. Radiat. Meas. 44, 472–476.
Grün, R., 2009b. The DATA program for the calculation of ESR age estimates on tooth enamel. Quatern. Geochronol. 4, 231–232.
Grün, R., Katzenberger-Apel, O., 1994. An alpha irradiator for ESR dating. Ancient TL 12, 35–38.
Grün, R., Schwarcz, H.P., Chadam, J.M., 1988. ESR dating of tooth enamel; coupled correction for U-uptake and U-series disequilibrium. Nucl. Tracks 14, 237–241.
Guerin, G., Mercier, N., Adamiec, G., 2011. Dose-rate conversion factors: update. Ancient TL 29, 5–8.
Hajraoui, M.A., 1994. L'industrie osseuse atérienne de la grotte d'el Mnasra. Préhist. Anthropol. Méditerr. 3, 91–94.
Henshilwood, C., Sealy, J., 1997. Bone artefacts from the Middle Stone Age at Blombos Cave, Southern Cape, South Africa. Curr. Anthropol. 38 (5), 890–895.
Henshilwood, C.S., Sealy, J.C., Yates, R., Cruz-Uribe, K., Goldberg, P., Grine, F.E., Klein, R.G., Poggenpoel, C., van Niekerk, K., Watts, I., 2001. Blombos Cave, Southern Cape, South Africa: preliminary report on the 1992–1999 excavations of the Middle Stone Age levels. J. Archaeol. Sci. 28, 421–448.
Higham, T., Compton, T., Stringer, C., Jacobi, R., Shapiro, B., Trinkaus, E., Chandler, B., Gröning, F., Collins, C., Hillson, S., O'Higgins, P., FitzGerald, P., Fagan, M., 2011. The earliest evidence for anatomically modern humans in northwestern Europe. Nature 479, 521–524.
Hublin, J.-J., 2000. Modern-non-modern hominid interactions: a Mediterranean perspective. In: Bar-Yosef, O., Pilbeam, D. (Eds.), The Geography of Neandertals and Modern Humans in Europe and the Greater Mediterranean, Peabody Museum of Archaeology and Ethnology, Peabody Museum Bulletin, 8, pp. 157–182. Harvard.
Hublin, J.-J., McPherron, S. (Eds.), 2011. Modern Origins: a North African Perspective. Springer, Berlin.
Hunt, C., Davison, J., Inglis, R., Farr, L., Simpson, D., el-Rishi, H., Barker, G., 2010. Site formation processes in caves: the Holocene sediments of the Haua Fteah, Cyrenaica, Libya. J. Archaeol. Sci. 37, 1600–1611.
Hunt, C., Reynolds, T.G., El-Rishi, H.A., Buzaian, A., Hill, E., Barker, G., 2011. Resource pressure and environmental change on the North African littoral:

Epipalaeolithic to Roman gastropods from Cyrenaica, Libya. Quatern. Int. 244, 15–26.
Inglis, R.H., 2012. Human occupation and changing environments during the Middle to Later Stone Age: Soil micromorphology at the Haua Fteah, Libya. Ph.D. Dissertation, University of Cambridge.
Iovita, R.P., 2009. Reevaluating connections between the Early Upper Palaeolithic of northeast Africa and the Levant: technological differences between the Dabban and the Emiran. In: Shea, J., Leiberman, D. (Eds.), Transitions in Prehistory: Papers in Honor of Ofer Bar-Yosef. Oxbow Books, Oxford, pp. 127–144.
Jackes, M., Lubell, D., 2008. Environmental and cultural change in the early and mid Holocene: evidence from the Télidjène basin, Algeria. Afr. Archaeol. Rev. 25, 41–55.
Jacobs, Z., Roberts, R.G., 2007. Advances in optically stimulated luminescence dating of individual grains of quartz from archaeological deposits. Evol. Anthropol. 16, 2100–2223.
Jacobs, Z., Duller, G.A.T., Wintle, A.G., 2006. Interpretation of single grain D_e distributions and calculation of D_e. Radiat. Meas. 41, 264–277.
Jacobs, Z., Meyer, M.C., Roberts, R.G., Adleias, V., Dibble, H., El Hajraoui, M.A., 2011. Single-grain OSL dating at La Grotte des Contrebandiers ('Smugglers' Cave'), Morocco: improved age constraints for the Middle Palaeolithic levels. J. Archaeol. Sci. 38, 3631–3643.
Jacobs, Z., Roberts, R.G., Nespoulet, R., El Hajraoui, M.A., Debénath, A., 2012. Single-grain OSL chronologies for Middle Palaeolithic deposits at El Mnasra and El Harhoura 2, Morocco: implications for Late Pleistocene human–environment interactions along the Atlantic coast of northwest Africa. J. Hum. Evol. 62, 377–394.
Karkanas, P., 2001. Site formation processes in Theopetra Cave: a record of climatic change during the Late Pleistocene and Early Holocene in Thessaly, Greece. Geoarchaeology 16, 373–399.
Kieffer, G., 1979. L'activité de l'Etna pendant les dernières 20000 ans. C. R. Acad. Sci. D 288, 1023–1026.
Klein, R., Scott, K., 1986. Re-analysis of faunal assemblages from the Haua Fteah and other late Quaternary sites in Cyrenaica. J. Archaeol. Sci. 37, 1600–1611.
Kuper, R., Kropelin, S., 2006. Climate-controlled Holocene occupation in the Sahara: motor of Africa's evolution. Science 313, 803–807.
Kuzucuoglu, C., Pastre, J.-F., Black, S., Ercan, T., Fontugne, M., Guillou, H., Hatté, C., Karabiyikoglu, M., Orth, P., Türkecan, A., 1998. Identification and dating of tephra layers from Quaternary sedimentary sequences of Inner Anatolia, Turkey. J. Volcanol. Geotherm. Res. 85, 153–172.
Linstädter, J., 2008. The Epipalaeolithic–Neolithic transition in the Mediterranean region of northwest Africa. Quartär 55, 41–62.
Lowe, J., Barton, R.N.E., Blockley, S.P.E., Bronk Ramsey, C., Cullen, V.L., Davies, W., Gamble, C., Grant, K., Hardiman, M., Housley, R., Lane, C.S., Lee, S., Lewis, M., MacLeod, A., Menzies, M., Müller, W., Pollard, A.M., Price, C., Roberts, A.P., Rohling, E.J., Satow, C., Smith, V.C., Stringer, C.B., Tomlinson, E.L., White, D., Albert, P., Arienzo, I., Barker, G., Carandente, A., Civetta, L., Ferrier, C., Guadelli, J.-L., Karkanas, P., Koumouzelis, M., Müller, U.C., Orsi, G., Pross, J., Rosi, M., Shalamanov-Korobar, L., Sirakov, N., Tzedakis, P.C., Boric, D., 2012. Volcanic ash layers illuminate the resilience of Neanderthals and early modern humans to natural hazards. Proc. Natl. Acad. Sci. 109, 13522–13537.
Macphail, R.I., Goldberg, P., 1999. The soil micromorphological investigation of Westbury Cave. In: Andrews, P., Stronger, C.B., Currant, A. (Eds.), Westbury Cave: the Natural History Museum Excavations 1976–1984. Western Academic and Special, Bristol, pp. 59–86.
McBurney, C.B.M., 1960. The Stone Age of Northern Africa. Penguin Books, London.
McBurney, C.B.M., 1967. The Haua Fteah in Cyrenaica and the Stone Age of the South-East Mediterranean. Cambridge University Press, Cambridge.
McBurney, C.B.M., Hey, R.W., 1955. Prehistory and Pleistocene Geology in Cyrenaican Libya. Cambridge University Press, Cambridge.
Mercier, N., Wengler, L., Valladas, H., Joron, J.L., Froget, L., Reyss, J.L., 2007. The Rhafas Cave (Morocco): chronology of the Mousterian and Aterian archaeological occupations and their implications for Quaternary geochronology based on luminescence (TL/OSL) age determinations. Quatern. Geochronol. 2, 309–313.
Mouralis, D., Pastre, J.F., Kuzucuoglu, C., Türkecan, A., Atici, Y., Slimak, L., Guillou, H., Kunesch, S., 2002. Les complexes volcaniques Rhyolithiques quaternaires d'Anatolie centrale (Göllü Dag et Acigöl, Turquie): genèse, instabilité, contraintes environnementales. Quaternaire 13, 219–228.
Moyer, C., 2003. The organisation of lithic technology in the middle and early Upper Palaeolithic industries at the Haua Fteah, Libya. Ph.D. Dissertation, University of Cambridge.
Nespoulet, R., El Hajraoui, M.A., Amani, F., Ben-Ncer, A., Débenath, A., El Idrissi, A., Lacombe, J.-P., Michel, P., Oujaa, A., Stroetzel, E., 2008. Palaeolithic and Neolithic occupations in the Témara region (Rabat, Morocco): recent data on hominin contexts and behavior. Afr. Archaeol. Rev. 25, 21–40.
North Greenland Ice Core Project members, 2004. High-resolution record of Northern Hemisphere climate extending into the last interglacial period. Nature 431 (7005), 147–151.
Olivieri, A., Achilli, A., Pala, M., Battaglia, V., Fornarino, S., Al-Zahery, N., Scozzari, R., Cruciani, F., Behar, D.M., Dugoujon, J.-M., Coudray, C., Sanatchiara-Benerecetti, A.S., Semino, O., Bandelt, H.-J., Torroni, A., 2006. The mtDNA legacy of the Levantine early Upper Palaeolithic in Africa. Science 314, 1767–1769.
Olley, J.M., Pietsch, T., Roberts, R.G., 2004. Optical dating of Holocene sediments from a variety of geomorphic settings using single grains of quartz. Geomorphology 60, 337–358.
Orsi, G., De Vita, S., Di Vito, M., 1996. The restless, resurgent Campi Flegrei nested caldera (Italy): constraints on its evolution and configuration. J. Volcanol. Geotherm. Res. 74, 179–214.
Osborne, A.H., Vance, D., Rohling, E., Barton, N., Rogerson, M., Fello, N., 2008. A humid corridor across the Sahara for the migration "out of Africa" of early modern humans 120,000 years ago. Proc. Natl. Acad. Sci. 105 (43), 16444–16447.
Pabst, S., Wörner, G., Civetta, L., Tesoro, R., 2008. Magma chamber evolution prior to the Campanian Ignimbrite and Neapolitan Yellow Tuff eruptions (Campi Flegrei, Italy). Bull. Volcanol. 70, 961–976.
Pereira, L., Silva, N.M., Franco-Duarte, R., Fernandes, V., Pereira, J.B., Costa, M.D., Martins, H., Soares, P., Behar, D.M., Richards, M.M., Macaulay, V., 2010. Population expansion in the North African Late Pleistocene signalled by mitochondrial DNA haplogroup U6. Evol. Biol. 10, 390.
Pickering, R., Hancox, P.J., Lee-Thorp, J.A., Grün, R., Mortimer, G.E., McCulloch, M., Berger, L.R., 2007. Stratigraphy, U–Th chronology, and paleoenvironments at Gladysvale Cave: insights into the climatic control of South African hominin-bearing cave deposits. J. Hum. Evol. 53, 602–619.
Rebollo, N.R., Weiner, S., Brock, F., Meignen, L., Goldberg, P., Belfer-Cohen, A., Bar-Yosef, O., Boaretto, E., 2011. New radiocarbon dating of the transition from the Middle to the Upper Paleolithic in Kebara Cave, Israel. J. Archaeol. Sci. 38, 2424–2433.
Reimer, P.J., McCormac, F.G., 2002. Marine radiocarbon reservoir corrections for the Mediterranean and Aegean Seas. Radiocarbon 44 (1), 159–166.
Reimer, P.J., Baillie, M., Bard, E., Bayliss, A., Beck, J.W., Blackwell, P.G., Bronk Ramsey, C., Buck, C.E., Burr, C.E., Edwards, R.L., Friedrich, M., Grootes, P.M., Guilderson, T.P., Hajdas, I., Heaton, T.J., Hogg, A.G., Hughen, K.A., Kaiser, K.F., Kromer, B., McCormac, F.G., Manning, S.W., Reimer, R.W., Richards, D.A., Southon, J.R., Talamo, S., Turney, C.S.M., van der Plicht, J., Weyhenmeyer, C.E., 2009. INTCAL09 and MARINE09 radiocarbon age calibration curves, 0–50,000 years cal BP. Radiocarbon 51, 1111–1150.
Reynolds, T., 2012. The Middle Palaeolithic of Cyrenaica: is there an Aterian at the Haua Fteah and does it matter? Quatern. Int. 300, 171–181.
Richter, D., Moser, J., Nami, M., Eiwanger, J., Mikdad, A., 2010. New chronometric data from Ifri n'Ammar (Morocco) and the chronostratigraphy of the Middle Palaeolithic in the Western Maghreb. J. Hum. Evol. 59, 672–679.
Rhodes, E.J., Bronk Ramsey, C., Outram, Z., Batt, C., Willis, L., Dockrill, S., Bond, J., 2003. Bayesian methods applied to the interpretation of multiple OSL dates: high precision sediment ages from Old Scatness Broch excavations, Shetland Isles. Quatern. Sci. Rev. 22, 1231–1244.
Ruhlmann, A., 1951. La Grotte Préhistorique de Dar es-Soltan. Institut des Hautes Études Marocaines, Larose, Paris, pp. 1–210.
Russell, N.J., Armitage, S.J., 2012. A comparison of single-grain and small aliquot dating of fine sand from Cyrenaica, northern Libya. Quatern. Geochronol. 10, 62–67.
Scerri, E., 2012. The Aterian and its place in the North African Middle Stone Age. Quatern. Int. 300, 111–130.
Schwenninger, J.-L., Collcutt, S.N., Barton, N., Bouzouggar, A., Clark- Balzan, L., El Hajraoui, M.A., Nespoulet, R., Debénath, A., 2010. A new luminescence chronology for Aterian cave sites on the Atlantic coast of Morocco. In: Garcea, E.A. (Ed.), South-Eastern Mediterranean Peoples between 130,000 and 10,000 Years Ago. Oxbow Books, Oxford, pp. 18–36.
Shea, J., 2010. Neanderthals and early *Homo sapiens* in the Levant. In: Garcea, E.A.E. (Ed.), South-Eastern Mediterranean Peoples between 130,000 and 10,000 Years Ago. Oxbow Books, Oxford, pp. 126–143.
Smith, T.M., Tafforeau, P.T., Reid, D.J., Grün, R., Eggins, S., Boutakiout, M., Hublin, J.-J., 2007. Earliest evidence of modern human life history in North African early *Homo sapiens*. Proc. Natl. Acad. Sci. 104, 6128–6133.
Stoops, G., 2003. Guidelines for Analysis and Description of Soil and Regolith Thin Sections. Soil Society of America Inc., Madison, Wisconsin.
Taborin, Y., 1993. La parure en coquillage au Paléolithique. In: XXIXe suppléments à Gallia Préhistoire. CNRS, Paris.
Taylor, R.M., 1982. Colour in soils and sediments – a review. In: van Olphen, H., Veniale, F. (Eds.), International Clay Conference 1981. Elsevier, Amsterdam, pp. 749–761.
Thomsen, K.J., Murray, A.S., Bötter-Jensen, L., 2005. Sources of variability in OSL dose measurements using single grains of quartz. Radiat. Meas. 39, 47–61.
Thomsen, K.J., Murray, A.S., Bötter-Jensen, L., Kinahan, J., 2007. Determination of burial dose in incompletely bleached fluvial samples using single grains of quartz. Radiat. Meas. 42, 370–379.
Tomlinson, E.L., Arienzo, I., Civetta, L., Wulf, S., Smith, V.C., Hardiman, M., Lane, C.S., Carandente, A., Orsi, G., Rosi, M., Müller, W., Menzies, M.A., 2012a. Geochemistry of the Phlegraean Fields (Italy) proximal sources for major Mediterranean tephras: implications for the dispersal of Plinian and co-ignimbritic components of explosive eruptions. Geochim. Cosmochim. Acta 93, 102–128.
Tomlinson, E.L., Kinvig, H.S., Smith, V.S., Blundy, J.D., Gottsmann, J., Müller, W., Menzies, M.A., 2012b. The Upper and Lower Nisyros Pumices: revisions to the Mediterranean tephrostratigraphic record using glass geochemistry. J. Volcanol. Geotherm. Res. 243–244, 69–80.
Trinkhaus, E., 2005. Early modern humans. A. Rev. Anthropol. 34, 207–230.
Vogel, J.C., Waterbolk, H.T., 1963. Groningen radiocarbon dates IV. Radiocarbon 5, 163–202.
Vogel, J.C., Waterbolk, H.T., 1967. Groningen radiocarbon dates VII. Radiocarbon 9, 107–155.
Volentik, A.C.M., Vanderkluysen, L., Principe, C., Hunziker, J.C., 2005. Stratigraphy of Nisyros Volcano (Greece). In: Hunziker, J.C., Marini, L. (Eds.), The Geology,

Geochemistry and Evolution of Nisyros Volcano (Greece). Implications for the Volcanic Hazards. Mém. Géol. 44, pp. 26–66.
Waelbroeck, C., Frank, N., Jouzel, J., Parrenin, F., Masson-Delmotte, V., Genty, D., 2008. Transferring radiometric dating of the last interglacial sea level high stand to marine and ice core records. Earth Planet. Sci. Lett. 265, 183–194.
Wengler, L., 2010. A new relationship between Mousterian and Aterian in North Africa. In: Conard, N.J., Delagnes, A. (Eds.), Settlement Dynamics of the Middle Paleolithic and Middle Stone Age, 3. Kerns Verlag, Tübingen, pp. 67–80.
Weninger, B., Alram-Stern, E., Bauer, E., Clare, L., Danzeglocke, U., Jöris, O., Kubatzi, C., Rollefson, G., Tordorova, H., van Ander, T., 2006. Climatic forcing due to the 8200 cal yr BP event observed at early Neolithic sites in the eastern Mediterranean. Quatern. Res. 66, 401–420.
Wood, R.E., Douka, K., Boscato, P., Haesaerts, P., Sinitsyn, A., Higham, T.F.G., 2012. Testing the ABOx-SC method: dating known age charcoals associated with the Campanian Ignimbrite. Quatern. Geochronol. 9, 16–26.
Woodward, J., Goldberg, P., 2001. The sedimentary records in Mediterranean rockshelters and caves: archives of environmental change. Geoarchaeology 16, 327–354.
Wrinn, P.J., Rink, W.J., 2003. ESR dating of tooth enamel from Aterian levels at Mugharet el'Aliya (Tangier, Morocco). J. Archaeol. Sci. 30, 2123–2133.
Wulf, S., Kraml, M., Brauer, A., Keller, J., Negendank, J.F.W., 2004. Tephrochronology of the 100 ka lacustrine sediment record of Lago Grande di Monticchio (southern Italy). Quatern. Int. 122, 7–30.
Wulf, S., Brauer, A., Mingram, J., Zolitschka, B., Negendank, J.F.W., 2007. Distal tephras in the sediments of Monticchio maar lakes. In: Principe, C. (Ed.), Geologia del Monte Vulture. Boll. Soc. Geol. Ital., 105–122.